BRAIN
ORIGINAL ARTICLE

Targeting aberrant dendritic integration to treat cognitive comorbidities of epilepsy

Nicola Masala,[1] Martin Pofahl,[1] André N. Haubrich,[1] Khondker Ushna Sameen Islam,[2] Negar Nikbakht,[1] Maryam Pasdarnavab,[1] Kirsten Bohmbach,[3] Kunihiko Araki,[1] Fateme Kamali,[1] Christian Henneberger,[3,4,5] Kurtulus Golcuk,[1] Laura A. Ewell,[1,6,7] Sandra Blaess,[2] Tony Kelly[1] and Heinz Beck[1,4]

Memory deficits are a debilitating symptom of epilepsy, but little is known about mechanisms underlying cognitive deficits. Here, we describe a Na^+ channel-dependent mechanism underlying altered hippocampal dendritic integration, degraded place coding and deficits in spatial memory.

Two-photon glutamate uncaging experiments revealed a marked increase in the fraction of hippocampal first-order CA1 pyramidal cell dendrites capable of generating dendritic spikes in the kainate model of chronic epilepsy. Moreover, in epileptic mice dendritic spikes were generated with lower input synchrony, and with a lower threshold. The $Na_v1.3/1.1$ selective Na^+ channel blocker ICA-121431 reversed dendritic hyperexcitability in epileptic mice, while the $Na_v1.2/1.6$ preferring anticonvulsant S-Lic did not. We used *in vivo* two-photon imaging to determine if aberrant dendritic excitability is associated with altered place-related firing of CA1 neurons. We show that ICA-121431 improves degraded hippocampal spatial representations in epileptic mice. Finally, behavioural experiments show that reversing aberrant dendritic excitability with ICA-121431 reverses hippocampal memory deficits.

Thus, a dendritic channelopathy may underlie cognitive deficits in epilepsy and targeting it pharmacologically may constitute a new avenue to enhance cognition.

1 Medical Faculty, Institute for Experimental Epileptology and Cognition Research, University of Bonn, 53127 Bonn, Germany
2 Neurodevelopmental Genetics, Institute of Reconstructive Neurobiology, Medical Faculty, University of Bonn, 53127 Bonn, Germany
3 Institute of Cellular Neurosciences, Medical Faculty, University of Bonn, 53127 Bonn, Germany
4 Deutsches Zentrum für Neurodegenerative Erkrankungen, 53127 Bonn, Germany
5 Department of Clinical and Experimental Epilepsy, Institute of Neurology, University College London, London WC1N 3BG, UK
6 Department of Anatomy and Neurobiology, University of California, Irvine, CA 92697-3950, USA
7 Center for the Neurobiology of Learning and Memory, University of California, Irvine, CA, 92697, USA

Correspondence to: Heinz Beck
Institute for Experimental Epileptology and Cognition Research
Venusberg-Campus 1, 53105 Bonn, Germany
E-mail: Heinz.Beck@ukb.uni-bonn.de

Correspondence may also be addressed to: Tony Kelly
E-mail: TKelly@uni-bonn.de

Keywords: epilepsy; dendritic integration; cognitive comorbidities; calcium imaging; dendritic spike

---

Received May 19, 2022. Revised November 18, 2022. Accepted November 22, 2022. Advance access publication November 30, 2022

Introduction

In most CNS pyramidal neurons, dendrites are capable of generating spikes in local membrane potential that are initiated by dendritic voltage gated Na^+ channels.[1] Because dendritic spikes are elicited by spatiotemporally clustered inputs, arising only if specific ensembles of presynaptic neurons are synchronously active, they have been proposed to endow neurons with the capability to act as input feature detectors.[2] Indeed, dendritic spikes have been found to be relevant for triggering place-related firing in CA1 neurons.[3,4] They thus constitute a key mechanism for dendritic integration and neuronal input–output computations, and have been strongly implicated in spatial navigation.

Dendritic spikes rely on targeted expression of voltage-gated ion channels in dendritic branches. In epilepsy, as well as in numerous other CNS disorders, the expression and function of ion channels are profoundly altered in CA1 neuron dendrites. In chronic epilepsy models, changes in K^+ channels,[5] T-type Ca^{2+} channels,[6,7] HCN channels[8,9] and Na^+ channels have been identified.[10] However, these studies have mainly focused on larger calibre, apical dendrites of pyramidal neurons, primarily because of the difficulties in obtaining direct patch-clamp recordings from thin dendrites. The integrative properties of thin, higher-order dendrites and how they change in chronic epilepsy have not been studied so far.

In this study, we address how dendritic integration via dendritic spikes is altered in chronic epilepsy, how this affects neuronal coding *in vivo* and how it impacts behaviour. We propose that an upregulation of Na^+ channels in hippocampal pyramidal neuron apical oblique dendrites underlies altered dendritic spikes, degraded place coding and cognitive deficits in experimental temporal lobe epilepsy (TLE).

Materials and methods

Animals

All experiments followed institutional guidelines of the Animal Care and Use committee of the University of Bonn. To avoid the documented sex differences in the severity of comorbidities and seizures in the kainate model of epilepsy [11,12] and thereby reduce animal numbers, all *in vitro*, and behavioural experiments were performed on C57BL/6J male wild-type mice (Charles River). For *in vivo* two-photon imaging experiments, we used male Thy1-GCaMP6 mice, which express GCaMP6s in most hippocampal neurons (C57BL/6J-Tg(Thy1-GCaMP6s)GP4.12Dkim/J; Jackson Lab Stock No.: 025776[13]). Mice were kept under a light schedule of 12 h on/12 h off, constant temperature of 22 ± 2°C and humidity of 65%. They had *ad libitum* access to water and standard laboratory food at all times. All efforts were made to minimize animal suffering and to reduce the number of animals used.

Kainate model of epilepsy

The kainate model of epilepsy was induced largely as described.[14] Specifically, for the experiments 5 week-old mice were injected with analgesic ketoprofen [Gabrilen, Mibe; 5 mg/kg body weight (b.w.); injection volume 0.1 ml/10 g b.w., s.c.] diluted in H_2O for injections (Ampuwa, Fresenius Kabi Deutschland) 30 min before injecting the anaesthetic. Mice were anaesthetized using a mixture of ketamine (Medistar; 80 mg/kg b.w.) and medetomidinhydrochloride (Domitor, Orion Pharma; 1.2 mg/kg b.w.; injection volume 0.1 ml/10 g, i.p.) and placed in a stereotaxic frame in a flat skull position. Eyes were covered with eye ointment (Bepanthen, Bayer) to prevent drying and body temperature was maintained at 37°C using a regulated heating plate (TCAT-2LV, Physitemp) and a rectal thermal probe. The surface was locally anaesthetized with a drop of 10% lidocaine and after 3–5 min residual soft tissue was removed from the skull bones with a scraper and 3% H_2O_2/NaCl solution. After complete drying, the cranial sutures were clearly visible and served as orientation for the determination of the drilling and injection sites. For stereotactic injection, a hole was carefully drilled through the skull with a dental drill, avoiding excessive heating and injury to the meninges. Any minor bleeding was stopped with a sterile pad. A stainless steel cannula (0.5 mm outer diameter) connected to a 10 µl microsyringe (Hamilton) was filled with a 20 mM kainic acid (KA) solution (Sigma) in 0.9% sterile NaCl (Fresenius Kabi Deutschland) and positioned above the right dorsal hippocampus (anteroposterior −1.9 mm; mediolateral −1.5 mm; dorsoventral, −1.7 mm) with bregma as a reference. Injections of dextran-biotin (50 nl) marker showed that these coordinates correspond to upper border of the CA1 region of the dorsal hippocampus. Once the cannula reached the correct depth, it was left in place for 2 min before beginning injection to allow for tissue adjustment. Mice were given injections for ∼2 min (20 nl/min) of 50 nl of the KA solution using a micropump (Micro4 Microsyringe Pump Controller, WPI) operating the microsyringe. After injection, the cannula was left in place for additional 2 min to avoid reflux of injected solution along the needle track. Sham-operated mice were given injections of 50 nl of 0.9% sterile NaCl, but were otherwise treated identically. In mice intended for two-photon *in vivo* imaging, an additional virus injection and placement of a head fixation was carried out (see below). Mice had their scalp incision sutured and their anaesthesia terminated with atipamezolhydrochloride (Antisedant, Orion Pharma; 2.5 mg/kg b.w.; injection volume 0.1 ml/10 g, i.p.). Diazepam (Ratiopharm, injection volume 0.15 ml/20 g, s.c.) was administered to all mice 4 h after the start of status epilepticus (SE) to terminate the convulsions. At the same time, mice were also injected with glucose monohydrate (Glucosteril, Fresenius Kabi Deutschland; injection volume 0.25 ml, s.c.). Mice were returned to their cages and kept on a heatpad until they woke from anaesthesia. After recovery from anaesthesia, the animals were kept under observation and were injected with the analgesic ketoprofen to alleviate pain for 4 days. After surgery mice were housed in individual cages. They were subsequently used for *in vitro* experiments 30 days after kainate/sham injection, or for *in vivo* two-photon imaging or behavioural experiments.

Slice preparation and patch-clamp recording

Mice were deeply anaesthetized with isoflurane and then decapitated. Brains were rapidly removed and placed in ice cold (<2°C) sucrose-based artificial CSF (sucrose-ACSF) containing (in mM): 60 NaCl, 100 sucrose, 2.5 KCl, 1.25 NaH_2PO_4, 26 $NaHCO_3$, 1 $CaCl_2$, 5 $MgCl_2$, 20 glucose. Slices of 300 µm were cut with a vibratome (Leica) and incubated in sucrose-ACSF at 35°C for 30 min. Subsequently, slices were transferred to a submerged holding chamber containing normal ACSF containing (in mM): 125 NaCl, 3.5 KCl, 1.25 NaH_2PO_4, 26 $NaHCO_3$, 2.6 $CaCl_2$, 1.3 $MgCl_2$, 15 glucose at room temperature. All extracellular solutions were equilibrated with 95% O_2 and 5% CO_2.

Selected CA1 cells were visualized with infrared oblique illumination optics and a water immersion objective (60×, 0.9 NA, Olympus) and somatic whole-cell current-clamp recordings were performed with a BVC-700 amplifier (Dagan Corporation). Data were filtered at 10 kHz and sampled at 50 kHz with a Digidata 1440 interface controlled by pClamp Software (Molecular Devices). Patch-pipettes were pulled from borosilicate glass (outer diameter 1.5 mm, inner diameter 0.8 mm; Science Products) with a Flaming/Brown P-97 Puller (Sutter Instruments) to resistances of 2–5 MΩ in bath and series resistances ranging from 8 to 30 MΩ. The standard internal solution contained (in mM): 140 K-gluconate, 7 KCl, 5 HEPES, 0.5 $MgCl_2$, 5 phosphocreatine, 0.16 EGTA. Internal solutions were titrated to pH 7.3 with KOH, had an osmolality of 295 mOsm, and contained 100 µM Alexa Fluor 594 (Invitrogen). Voltages were not corrected for the calculated liquid-junction potential of +14.5 mV. Membrane potential was adjusted to −75 mV for all recordings. To assess somatic action potential firing, current steps (800 ms) of increasing amplitudes were injected via the somatic patch pipette. The analysis of the effects of S-Lic or ICA-121431 on maximal firing rates was done by identifying the current injection at which maximal firing rates were obtained under control conditions. Effects of drugs and washout were quantified using this current injection magnitude. Passive membrane properties, action potential properties and firing patterns were assessed throughout the entire course of the experiment. Cells with unstable input resistances or lacking overshooting action potentials were discarded as well as recordings with holding currents >–200 pA for 60 mV and access resistances >30 MΩ.

For AMPA receptor-mediated miniature excitatory postsynaptic current (mEPSC) recordings, the Na^+ channel blocker tetrodotoxin (1 µM) and $GABA_A$ receptor antagonist bicuculline (20 µM) were added to the extracellular ACSF at least 15 min before starting recordings. Cells were voltage clamped at −60 mV and synaptic currents were recorded with an Axopatch 200-B amplifier (Axon Instruments), filtered at 2 kHz and digitized at 5 kHz. Analysis was performed with Minianalysis.

In vitro two-photon uncaging

Two-photon glutamate uncaging at apical oblique dendrites of CA1 was performed using a dual galvanometer based scanning system (Prairie Technologies) to photo-release glutamate at multiple dendritic spines of CA1 neurons. MNI-caged-L-glutamate 15 mM (Tocris Cookson) was dissolved in HEPES-buffered solution (in mM as follows: 140 NaCl, 3KCl, 1.3 $MgCl_2$, 2.6 $CaCl_2$ 20 D-glucose and 10 HEPES, pH 7.4 adjusted with NaOH, 305 mOsmol/kg) and was applied using positive pressure via glass pipettes (<1 MΩ) placed in closed proximity to the selected apical oblique dendrites of CA1 neurons. We used two ultrafast laser beams of Ti:sapphire pulsed lasers (Chameleon Ultra, Coherent) tuned at 860 nm to excite the Alexa 594 and one tuned to 720 nm was used to photo-release at 10–15 dendritic spines (within ∼10 µm in length). The intensity of each laser beam was independently controlled with electro-optical modulators (Conoptics Model 302RM). MNI-glutamate was uncaged at increasing number of spines (2–15) with 0.5 ms exposure times and the laser was rapidly moved from spine to spine with a transit time of ~0.1 ms. The laser power at the slice surface was kept below 22 mW to avoid photo damage. The glutamate was uncaged onto a sequence of single spines to evoke unitary excitatory postsynaptic potential (uEPSP). To quantify deviations from linearity in dendritic integration, the arithmetic summation calculated from each individual uEPSP was compared to the actually measured EPSP during glutamate uncaging onto the same sequence of spines. The rate of rise of the dendritic spike initial fast phase was calculated from the maximum dV/dt value from dendritic spikes generated at similar number of spines (sham-control versus epileptic, 9.81 ± 0.31 and 9.51 ± 0.29 stimulated spines). The slow-phase NMDA area was calculated from the same dendritic spikes used to quantify dV/dt. The dendritic spike threshold was calculated as the amplitude of the expected EPSP at which dendritic spikes first occurred. All data analyses were done with Clampfit 9.2 software (Molecular Devices), IGOR Pro (Wavemetrics) and GraphPad Prism (GraphPad Software).

In vitro pharmacology

S-Lic was kindly supplied by Bial–PORTELA & CA. S-Lic or ICA-121431 (Tocris) were dissolved in dimethyl sulphoxide (DMSO), with a 0.1% concentration of DMSO in ACSF. Control ACSF contained concentrations of DMSO equivalent to the drug-containing solution. Drug effects were analysed 15 min after initiating the drug application. We selected the S-Lic concentrations (300 µM) to be at the high end of effective therapeutic concentrations reported in mouse models and patients.[15,16] This concentration of S-Lic reported maximally blocks Na^+ current amplitude recorded in isolated hippocampal neurons and Na^+ currents mediated by $Na_v1.2$ and $Na_v1.6$ channels expressed in heterologous expression systems.[17] Of note, this therapeutically relevant concentration failed to affect $Na_v1.1$ and $Na_v1.3$, which were insensitive to S-Lic at concentration up to 1000 µM.[15] ICA-121431 is a highly selective and potent inhibitor of $Na_v1.3$ and $Na_v1.1$ with reported IC_{50} values of 13 and 23 nM. We selected a concentration of 100 nM to maximally inhibit $Na_v1.3$ channels ($Na_v1.3$-mediated currents were inhibited by 80% at 100 nM) while still being selective for $Na_v1.3/1.1$ channels.[18] Branch strength plasticity induced by repetitive stimulations of dendritic spines[2,19] potentiated dendritic spike strength during the 15 min timeframe of our pharmacology experiments and precluded an examination of Na_v channel blocker on the dendritic spike inactivation and input synchrony.

Virus injections and head fixation

For Thy1-GCaMP6s mice intended for *in vivo* two-photon imaging experiments, injection of an adeno-associated virus (AAV) leading to labelling of astrocytes with mCherry (rAAV2/1.GFAP.mCherry, total volume 250 nl, 20 nl/min) was carried out in addition for improved motion correction using an orthogonal imaging channel. Following virus injection, Optibond (Optibond™ 3FL; two component, 48% filled dental adhesive, bottle kit; Kerr) was applied thinly to the skull to aid adhesion of dental cement. Subsequently, a flat custom-made head post ring was applied with the aid of dental cement (Tetric Evoflow) and the burrhole was closed.

Two-photon *in vivo* imaging, window implantation procedure

Cranial window surgery was performed to allow imaging from the dorsal hippocampal CA1 region. Thirty minutes before induction of anaesthesia, the analgesic buprenorphine was administered for analgesia (Buprenovet, Bayer; 0.05 mg/kg body weight; injection volume 0.1 ml/20 g b.w., i.p.), and dexamethasone (Dexa, Jenapharm; 0.1 mg/20 g body weight; injection volume 0.1 ml/20 g body weight, i.p.) and ketoprofen (Gabrilen, Mibe; 5 mg/kg body weight; injection volume 0.1 ml/10 g body weight, s.c.) were given to inhibit inflammation/swelling and pain. Mice were anaesthetized with 3–4% isoflurane in an oxygen/air mixture (25%/75%) and then placed in a stereotactic frame. Eyes were covered with eye ointment (Bepanthen, Bayer) to prevent drying and body temperature was maintained at 37°C using a regulated heating plate (TCAT-2LV, Physitemp) and a rectal thermal probe. Further anaesthesia was carried out via a mask with a reduced isoflurane dose of 1–2% at a gas flow of about 0.5 ml/min. A circular craniotomy (Ø 3 mm) was opened within the head fixation ring above the right hemisphere hippocampus using a dental drill. Cortical tissue was aspirated until the alveus fibres above CA1 became visible. A custom-made cone-shaped silicon inset (upper diameter 3 mm, lower diameter 2 mm, length 1.5 mm, RTV 615, Movimentive) attached to a cover glass (Ø 5 mm, thickness 0.17 mm) was inserted and fixed with dental cement. Postoperative care included analgesia by administering buprenorphine twice daily (Buprenovet, Bayer; 0.05 mg/kg body weight; injection volume 0.1 ml/20 g b.w., i.p.) and ketoprofen once daily (Gabrilen, Mibe; 5 mg/kg body weight; injection volume 0.1 ml/10 g body weight, s.c.) on the 3 consecutive days after surgery. Animals were carefully monitored twice daily on the following 3 days and recovered from surgery within 24–48 h, showing normal activity and no signs of pain.

Two-photon *in vivo* Ca^{2+} imaging

We used a commercially available two-photon microscope (A1 MP, Nikon) equipped with a 25 × long-working-distance, water-immersion objective (NA = 1, WD = 4 mm, XLPLN25XSVMP2, Olympus) controlled by NIS-Elements software (Nikon). GCaMP6s was excited at 940 nm using a Ti:sapphire laser system (~60 fs laser pulse width; Chameleon Vision-S, Coherent) and a fibre laser system at 1070 nm (55 fs laser pulse width; Fidelity-2, Coherent) to excite mCherry (see Supplementary Fig. 6). Emitted photons were collected using gated GaAsP photomultipliers (H11706–40, Hamamatsu). Movies were recorded using a resonant scanning system at a frame rate of 15 Hz and duration of 20 min per movie.

Habituation and behaviour on the linear track

Experiments were performed in head-fixed awake mice running on a linear track. Two weeks before the measurements, mice were habituated to the head fixation. Initially mice were placed on the treadmill without fixation for 5 min at a time. Subsequently, mice were head-fixed, but immediately removed if signs of fear or anxiety were observed. These habituation sessions lasted 5 min each and were carried out three times per day, flanked by 5 min of handling. During the following 3–5 days, sessions were extended to 10 min each. All experimental recordings were from experimental sessions of 20 min duration. After habituation, mice ran well on the treadmill for average distances between 9 and 27 m per 20-min session (see Supplementary Fig. 6C and D). The treadmill we implemented was a self-constructed linear horizontal treadmill, similar to Royer *et al.*[20] The belt surface was equipped with tactile cues (see Supplementary Fig. 6B). Belt position and running speed were measured by modified optical mouse sensors. All stimulation and acquisition processes were controlled by custom-made software written in LabView. Detailed construction plans and LabView software are available upon request.

Data analysis, two-photon imaging

All analyses on imaging data and treadmill behaviour data were conducted in MATLAB using standard toolboxes, open access toolboxes and custom-written code. To remove motion artefacts, recorded movies were registered using a Lucas–Kanade model.[21] In most cases, the red (mCherry) channel was used for motion correction. Individual cell locations and fluorescence traces were identified using a constrained non-negative matrix factorization-based algorithm and afterwards Ca^{2+} events were identified with a deconvolution algorithm.[22] All components were manually inspected and only those kept that showed shape and size of a CA1 pyramidal neuron and at least one Ca^{2+}-event amplitude three standard deviations (SD) above noise level in their extracted fluorescence trace. We binarized individual cell fluorescence traces by converting the onsets of detected Ca^{2+} events to binary activity events.

Spatial tuning

To address spatial tuning of CA1 pyramidal neurons we used spatial tuning vector analysis.[23] We restricted analysis to running epochs, where a running epoch was defined as an episode of movement with a minimal duration of 2.5 s above a threshold of 4 cm/s in a forward direction. Only cells with four or more event onsets during all running epochs in a 20 min session were included in the analysis. Mouse position was represented as vectors pointing towards the position on the linear track occupied by the mouse. We calculated the mean of the vectors at the times of all transient onsets during a session, weighted by the time spent in that bin. We addressed statistical significance by creating the null distribution for every spatially tuned cell. This was achieved by randomly shuffling the onset times and recalculating the spatial tuning vector 1000 times. The P-value was calculated as the percentage of vector lengths arising from the shuffled distribution that was larger than the actual vector length.

Detection of aberrant synchronized activity during two-photon imaging

In order to detect and further analyse aberrant activity in the two-photon Ca^{2+} imaging data, we used a custom-written pipeline in Python, mainly using the computer vision library OpenCV. After importing the movies into our pipeline, the median image obtained from 100 randomly selected frames is set to be the background frame. In the next step, while iterating through all frames, each frame is converted to greyscale and is convolved with a Gaussian kernel of size 35 × 35 pixels. The estimated background frame is then subtracted from all frames. To define a detection threshold for the aberrant activity episodes, the SD of the pixel intensities are calculated for each frame of the movie. The 95th percentile of the resulted distribution was taken as an intensity threshold for creating a binary segmented image. The aberrant activity episodes were then detected by searching the binary images for contours. If the size of a detected contour was comparable to the average size of somata in our field of view, this contour was excluded. The duration of activity epochs was calculated from the time stamp of the start and the end frame of the detected activity.

Histochemistry

To verify successful viral transduction and window position, animals were deeply anaesthetized with ketamine (80 mg/kg b.w.) and xylazine (15 mg/kg b.w.). After confirming a sufficient depth of anaesthesia, mice were heart-perfused with cold phosphate-buffered saline (PBS) followed by 4% paraformaldehyde (PFA) in PBS. Animals were decapitated and the brain removed and stored in 4% PFA in PBS solution for 24 h. Coronal slices of the hippocampus 50–70-µm thick were cut on a vibratome (Leica). For nuclear staining, brain slices were kept for 10 min in a 1:1000 DAPI solution at room temperature. Brain slices were mounted and the red, green and blue channel successively imaged under an epi fluorescence or spinning disc microscope (Visitron VisiScope).

In vivo pharmacology

In vivo treatment with the selective $Na_v1.3$ antagonist ICA-121431 for behavioural experiments and *in vivo* two-photon imaging was carried out at a dose of 0.5 mg/kg body weight. ICA-121431 was solubilized in distilled water and applied via gavage with a stainless steel gavage cannula (20 G, 30 mm long, FST).

Behaviour, object location, object recognition memory and Y-maze spontaneous alternation task

Three weeks after kainate/sham treatment, mice were habituated to handling by the experimenter for 10 min daily on two consecutive days prior to starting behavioural experiments. On experimental days, mice were moved from the animal holding facility to the experimental room at least 45 min before starting the experiments. The experimental room was quiet and had dim light conditions of around 20 lux, achieved by a single light spot pointed towards the ceiling. Object location and object recognition experiments took place in the same acrylic glass arena that was 56 cm × 36 cm in size and had 20 cm high transparent walls without internal visual cues. Between animals, the arena was thoroughly cleaned using 70% ethanol. The arena was placed on an infrared light board and animal activity was monitored with an infrared camera above the arena and animal tracking software (Noldus × 8.5, Ethovision). On the first three consecutive days, mice were placed in the empty arena for 10 min. After 2 days of break, treatment was started by administering animals twice per day via gavage with the drug or control substance. Animals received either 0.5 mg/kg body weight of ICA-121431 dissolved in water (Ampuwa) or plain water, 4 and 2 h before starting experiments on every experimental day. On the first day of treatment, mice were again placed in the empty open field arena for 10 min (Day 4 of open field; see Fig. 7A). On the next day, mice were introduced to two identical objects (blue beaker bottle caps, diameter 5.5 cm) placed on opposite ends of a narrow side of the arena, 11.5 cm away from the walls, for 10 min (Habituation; see Fig. 7A). Twenty-four hours later, one of the objects was displaced along the long side of the arena by 32 cm and mice were given 5 min to explore [object location memory (OLM) test; see Fig. 7A]. On the next day, mice encountered the objects in the same position for 10 min as the day before to habituate them to the displacement (Habituation, Day 7, see Fig. 7A). Twenty-four hours later, a novel object, a transparent Petri dish of the same diameter, replaced one of the familiar objects and mice were given 5 min to explore [novel object recognition (NOR) test; see Fig. 7A]. In separate experiments, we found that naïve mice on average do not express a preference for either object before learning (data not shown).

As an indicator of successful memory formation and recall, we compared exploration times of the objects. Successful memory formation is indicated by an increased exploration of the displaced or novel object compared to the familiar object. We computed a discrimination index percentage according to the following formula (exploration time of displaced/novel object − exploration time of familiar object)/(exploration time of displaced/novel object + exploration time of familiar object) × 100. Exploration times were manually scored by an experienced observer blinded to the treatment condition of the animal. We considered exploration when the nose of the animal was apposed to the object and pointed towards it. Time spent climbing onto the object was not considered exploration. We excluded trials in which mice did not explore the objects for more than 3 s in both the habituation and recall trials, and if mice displayed a strong preference towards one of the two objects in habituation trials, indicated by a discrimination index (%) of >20. Occupancy plots were created using a custom-written MATLAB script using tracking data from the Noldus software.

To investigate spatial working memory, the mice were placed for 10 min in a Y-shaped arena made of red Plexiglas with three arms (40 cm long, 8 cm wide) arranged at 120° angles. Symbols glued to the end of the arms served as internal visual cues. Spontaneous alternation behaviour was analysed by manually counting the number of three consecutive entries into different arms and dividing it by the number of potential alternations according to the following formula: number of successful alternations/(total arm entries − 2). Arm entries were scored when all four paws of an animal were in an arm.

Chronic local field potential monitoring

Five male C57BL/6J mice (age 13 weeks, Charles River) were induced with kainate according to the methods described above except that a 10 µl Nanofil syringe (World Precision Instruments) was used and the kainate injection coordinate was [−1.9 mm AP, 1.5 mm ML (right side), −1.1 mm DV from bregma]. Seven weeks after status, mice were implanted with microdrives comprising movable tungsten electrodes. Mice were injected with the analgesic buprenorphine a (0.05 mg/kg b.w.) and anaesthetized with 1–2% isoflurane. Mice were fixed in a stereotactic frame and the microdrive was implanted above the right hippocampus (−2 mm AP, 1.5 mm ML). Reference and ground screws were implanted anterior to bregma. The implant was fixed to the skull with stainless screws and dental cement. Two weeks after implantation, local field potential (LFP) was recorded from the hippocampus of mice for 8 days (1 h each day) using a Neuralynx system (Digital Lynx SX, sample rate: 32 kHz, filter: 1–8000 Hz) and Cheetah 6.4.1. Animals were video monitored during the LFP recording. Seizures were detected in LFP recordings using a home-written MATLAB code. First LFP was band pass filtered (1–300 Hz). In order to detect the ictal spikes a threshold was defined manually by the user (2–4 SD > mean of full recording). Peaks that were bigger than threshold were categorized as spikes. Ictal spikes that were <2 s to the previous spikes were grouped together as one ictal event (seizure). Seizures closer than 5 s were merged together and counted as one seizure. Only seizures that lasted for at least 10 s were counted. Video observation facilitated defining seizure as subclinical or behavioural.

Multiplex fluorescent *in situ* hybridization (RNAscope)

Multiplex fluorescent RNA *in situ* hybridization was performed on 40 µm fixed, frozen hippocampal sections using RNAscope Fluorescent Multiplex Detection Reagents v2 (323110, ACDBio) according to the instructions provided by the manufacturer for fixed-frozen tissue (User Manual: 323100-USM). Hybridized target probes were lableled by TSA Plus Cyanine 3 and TSA Plus Cyanine 5 (NEL760001KT, Perkin Elmer). The probes *Scn3a* (Mm-Scn3a, Cat No. 502 641), *Gad1* (Mm-Gad1-C3, Cat No. 400951-C3) and *Gad2* (Mm-Gad2-C2, Cat No. 439371-C2) were designed by ACDBio. Sections were counterstained with DAPI (Cat No. 323108, ACDBio), then mounted with Aqua Polymount (Polysciences Inc.). *In situ* hybridized sections were imaged at an inverted Zeiss AxioObserver equipped with a CSU-W1 confocal scanner unit (50 µm pinhole disk, Yokogawa). At ×40 (C-Apochromat, 40×/1.2 water, Zeiss) magnification, tile images and z-stacks were acquired with laser lines 405, 488 and 561 nm. Images taken with the 40× objective are maximum intensity projections of z-stacks. Tile images were stitched with VisiView software (Visitron Systems). The anatomical region corresponding to the pyramidal layer of hippocampal CA1 was manually outlined in Fiji (https://fiji.sc/), based on the Allen Mouse Brain Reference Atlas. A binary mask of *Gad1/2* probe-expressing cells was created in Fiji to segment GABAergic neurons and non-GABAergic pyramidal cells of CA1 and analyse them separately. For quantification, a non-biased automated approach was used to detect and quantify probe signals using the open-source image analysis software CellProfiler.[7] The CellProfiler pipeline 'Speckle Counting' (http://cellprofiler.org/examples/#Speckles) was optimized to detect nuclei and probe signals (punctae). A threshold was set at 5 SD above mean pixel intensity and probe signals above the threshold were assigned to the closest nucleus and punctae located within the nuclei were quantified.

Immunoblotting

For Western blots, CA1 hippocampal regions were harvested from sham-control and epileptic brains. The tissue was homogenized with RIPA buffer (182–02451, Wako) containing 10% protease inhibitors (4693116001, Roche) and phosphatase inhibitors (4906845001, Roche). Homogenates were subsequently incubated on ice for 20 min and centrifuged for 10 min at 4°C. The lysates were mixed with 4 × NuPAGE LDS sample buffer (NP0008, Novex) and heated at 95°C for 5 min. After denaturation, each lysate was separated by sodium dodecyl sulphate–polyacrylamide gel electrophoresis (SDS-PAGE; 8%) and subsequently transferred to a nitrocellulose membrane, which was blocked in 5% milk. The primary and secondary antibodies were the following: anti-$Na_v1.2$ rabbit polyclonal (1:200; ASC-002, Alomone Labs); anti-$Na_v1.3$ rabbit polyclonal (1:200; ASC-004, Alomone Labs); anti-GAPDH mouse monoclonal (1:1000, NB300-221, Novus); IRDye® 800CW goat anti-rabbit IgG secondary antibody (1:10000, 926-32211, LI-COR Biosciences); IRDye® 680LT donkey anti-mouse IgG secondary antibody (1:10000, 926-68022, LI-COR Biosciences).

The primary antibodies were incubated for 2 h at room temperature (RT), while the fluorescently labelled IRDye anti-rabbit 800 nm IgG (LI-COR Biosciences) or IRDye anti-mouse 680 nm were incubated for 45 min at RT and detected with the infrared Odyssey system (LI-COR Biosciences). Band intensity was quantified by Image Studio Lite 5.2 software (LI-COR Biosciences). The Na_v protein band intensity was determined as a ratio of the housekeeping protein glycerinaldehyde-3-phosphate-dehydrogenase (GAPDH) within the same immunoblot and normalized to the average ratio obtained in sham-control.

Histopathology

Histopathological evaluation in the kainic acid model was performed on 40 µm fixed, frozen hippocampal slices. Sections were counterstained with DAPI (Cat No. 323108, ACDBio), then mounted with Aqua Polymount (Polysciences Inc.). The thickness of the CA1, CA3 and DG layers was measured in Fiji. For the CA1 region, the layer thickness was obtained by averaging five points 300 µm equally distant, between proximal and distal CA1, based on the Allen Mouse Brain Reference Atlas. For CA3, dorsal DG and ventral DG, the thickness was obtained by averaging three points 300 µm equally distant.

Statistics

Average values in the text and figures are expressed as mean ± SEM. Significance level was set to $P < 0.05$. Detailed statistics are described for each individual test performed in the text.

Data availability

The data that support the findings of this study are available from the corresponding author, upon reasonable request.

Results

Altered dendritic integration via dendritic spikes in chronic epilepsy

We examined dendritic integration in the kainate model, a well-established model of chronic temporal lobe epilepsy,[14,24,25] characterized by spontaneous recurrent seizures (Supplementary Fig. 1A–C) and hippocampal pathology (Supplementary Fig. 1D–I). The intrinsic firing properties of neurons showed an increased action potential output (Supplementary Fig. 1J–N), as well as an increased fraction of bursting neurons, similar to other mouse TLE models[6] (Supplementary Fig. 1M, N and Supplementary Table 1).

To probe dendritic integration in CA1 pyramidal neurons we used two-photon glutamate uncaging.[1,26] Responses of single spines to uncaging of glutamate (uEPSPs) were calibrated to ∼1 mV in both sham-control and epileptic animals (1.09 ± 0.42 mV, $n = 98$ versus 1.07 ± 0.04 mV, $n = 85$ dendrites, unpaired *t*-test, $P = 0.80$; Supplementary Fig. 2A–C). The rise and decay kinetics of such single-spine unitary EPSPs elicited by uncaging were slightly but significantly faster in epileptic animals (Supplementary Fig. 2D and E). This was also observed in mEPSC recordings (Supplementary Fig. 2F–K). Spine density in first- and second-order dendrites did not differ between sham-controls and epileptic animals (Supplementary Fig. 2L–N).

We then went on to probe the capability of CA1 dendrites to generate dendritic spikes by stimulating multiple spines quasi-synchronously (interspine stimulation interval, 0.1 ms). As described previously,[1,26] CA1 dendrites either displayed linear integration only, or were capable of generating sudden supralinear dendritic spikes when increasing numbers of spines were synchronously stimulated (representative examples in Fig. 1A–C). In linearly integrating dendritic branches, the linear summation of single spine uEPSPs was augmented in epileptic animals in first-order branches emanating from the main dendritic shaft ($n = 35$ and 26 in sham-control versus epileptic mice). Linearly integrating second-order dendrites did not show differences in EPSP summation [Fig. 1D and F, $n = 23$ and 15 in sham-control versus epileptic mice, two-way ANOVA main effect, sham-control versus epileptic mice: $F(1,95) = 7.38$, $P = 0.0078$; first order versus second order: $F(1,95) = 4.33$, $P = 0.040$; interaction: $F(1,95) = 0.32$, $P = 0.57$; Bonferroni's post-test, first-order dendrites sham-control versus epileptic mice $P = 0.018$; second-order dendrites sham-control versus epileptic mice $P = 0.35$; Supplementary Fig. 2O].

The difference in linear summation was normalized by application of the Na^+ channel blocker tetrodotoxin (TTX), indicating that it is caused by increases in voltage-gated Na^+ currents [Supplementary Fig. 3; sham-control and epileptic $n = 7$ and 6, respectively, two-way repeated measures ANOVA main effect, sham-control versus epileptic: $F(1,11) = 0.88$, $P = 0.37$; ACSF versus TTX: $F(1,11) = 26.96$, $P = 0.0003$; interaction: $F(1,11) = 10.15$, $P = 0.0087$; Bonferroni's post-test, ACSF versus TTX in epileptic $P = 0.0003$].

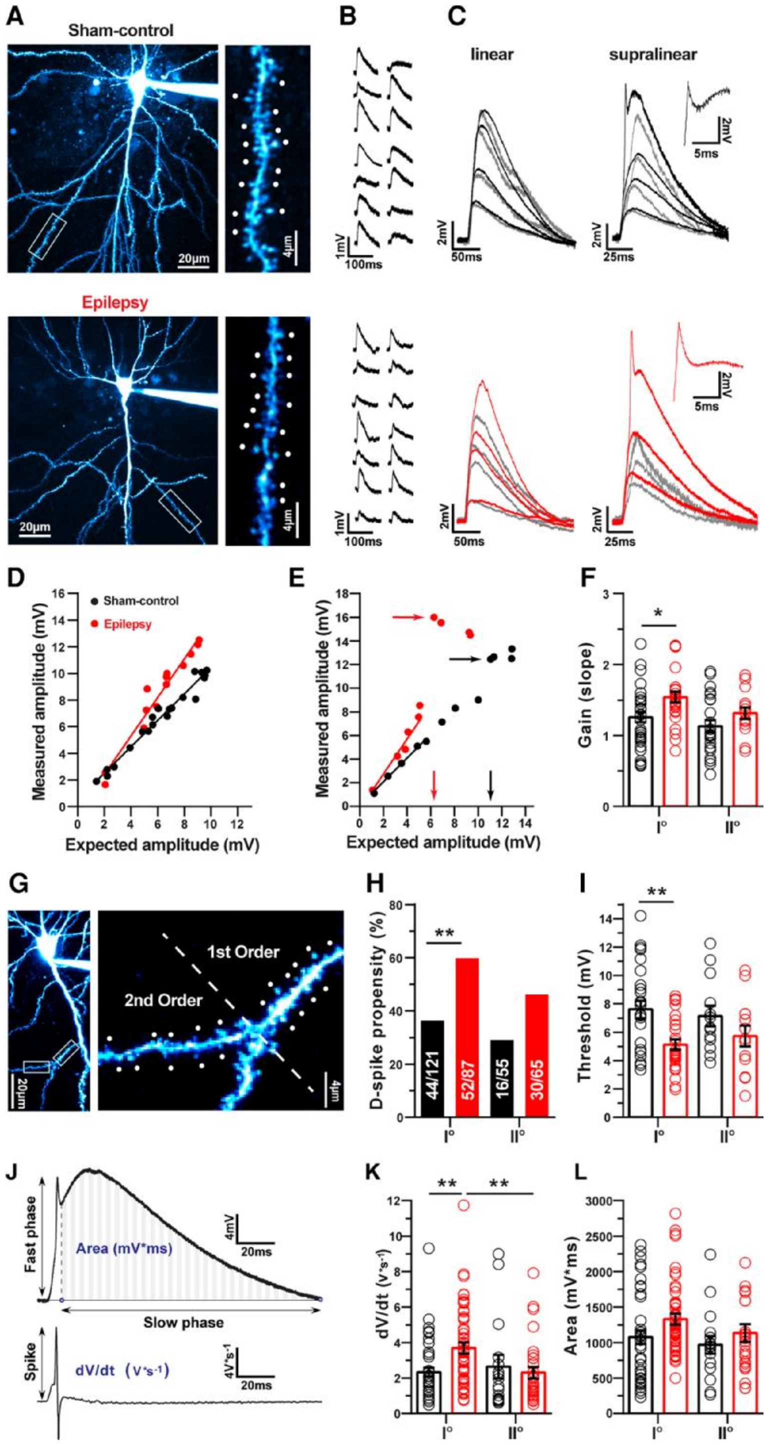

Figure 1 Probing dendritic integration in chronic epilepsy (kainate model of epilepsy). (**A**) CA1 pyramidal neurons filled with a fluorescent dye via the somatic patch recording pipette, close up of a dendritic segment with uncaging targeting points at spines. (**B**) Responses to single-spine stimulation with 2P-uncaging of MNI-glutamate measured with somatic patch recording. (**C**) Representative recordings of compound linear and supralinear EPSPs. Grey lines are expected EPSPs from linear summation of single spine responses. Examples of a branch with linear integration (*left*) and a branch capable of supralinear integration (*right*) are shown for sham-control (black) and epileptic mice (red). (**D**) Examples of linearly integrating first-order dendrites in sham-control (black) and epileptic animals (red). (**E**) Examples of first-order dendrites capable of generating supralinear dendritic spikes in sham-control (black) and epileptic animals (red). Occurrences of dendritic spikes and their voltage thresholds are indicated with arrows. (**F**) Quantification of the slope of the linear phase in linearly integrating first- and second-order dendrites in sham-control (black) and epileptic mice (red). Asterisks indicate Bonferroni's post-tests $P = 0.0176$. (**G**) Representative dendrite with first- and second-order branches. (**H**) The propensity for dendritic spikes is enhanced in first-order dendrites in epileptic animals (red) compared to sham-controls (black). Asterisks indicate Fisher's exact test $P = 0.0011$. (**I**) The threshold for generation of dendritic spikes, measured as indicated with arrows in **E** is reduced in first-order dendrites of epileptic animals, but not in second-order dendrites. Asterisks indicate Bonferroni's post-test, $P = 0.0017$. (**J**–**L**) The fast phase of dendritic spikes is accelerated in first-order dendrites from epileptic mice (**K**, asterisks indicate Bonferroni's post-test, rate of rise in first-order dendrites in sham-control versus epileptic $P = 0.0025$; first- versus second-order dendrites rate of rise in epileptic $P = 0.0074$). The area of the slow phase was unchanged.

Strikingly, the fraction of dendrites capable of generating dendritic spikes was significantly increased in first-order dendrites, but not in second-order dendrites in epileptic animals (Fig. 1E, G and H, first-order dendrites 36% versus 60%, Fisher's exact test $P = 0.0011$, second-order dendrites 29% versus 46%, Fisher's exact test $P = 0.062$). In these experiments, the average distances of the uncaging sites from the somatic region were not different when comparing sham-control and epileptic mice (first-order dendrites sham-control 66.2 ± 2.2 µm, $n = 101$ versus epileptic mice 64.9 ± 2.3 µm, $n = 69$; second-order dendrites sham-control 77.5 ± 2.6 µm, $n = 54$ versus epileptic mice 80.6 ± 2.8 µm, $n = 55$; unpaired Student's *t*-test first-order sham-control versus epileptic mice $P = 0.68$; second-order sham-control versus epileptic mice $P = 0.43$).

We next compared the properties of dendritic spikes in those branches capable of generating them. The threshold for generation of dendritic spikes was computed by determining the expected somatic voltage at which a dendritic supralinearity first occurred (indicated by arrows at the *x*-axis; Fig. 1E and Supplementary Fig. 2P). In epileptic animals, the voltage threshold to generate dendritic spikes was significantly reduced in first-order but not second-order dendrites [Fig. 1I; first-order dendrites $n = 25$ and 27, second-order dendrites $n = 13$ and 13 for sham-control and epileptic mice, respectively, two-way ANOVA main effect, sham-control versus epileptic: $F(1,74) = 9.92$, $P = 0.0024$; first-order versus second-order: $F(1,74) = 0.012$, $P = 0.91$; interaction: $F(1,74) = 0.77$, $P = 0.38$; Bonferroni's post-test, threshold in first-order dendrites in sham-control versus epileptic $P = 0.0017$].

The reduction was remarkably pronounced in some first-order dendrites from epileptic animals, with dendritic spikes sometimes being generated with stimulation of as few as 1–3 spines, and somatic voltages of as little as ~3 mV (see Supplementary Fig. 4 for dendritic spike elicited with a single spine stimulation).

A further characteristic of dendritic spikes is the rate of rise of the initial fast phase, which reflects the contribution of voltage-gated sodium channels. The maximal rate of rise was determined from the first derivation of the voltage trace (indicated in Fig. 1J). In first-order dendrites, but not second-order dendrites, we observed a significant increase in the maximal rate of rise in epileptic animals [Fig. 1K; first-order dendrites $n = 44$ and 52, second-order dendrites $n = 16$ and 30 in sham-control and epileptic, respectively, two-way ANOVA main effect, sham-control versus epileptic: $F(1,139) = 1.86$, $P = 0.18$; first-order versus second-order: $F(1,139) = 1.96$, $P = 0.16$; interaction: $F(1,139) = 5.08$, $P = 0.025$; Bonferroni's post-test, rate of rise in first-order dendrites in sham-control versus epileptic $P = 0.0025$; first- versus second-order dendrites rate of rise in epileptic $P = 0.0074$]. In contrast to the fast phase of the dendritic spikes, the subsequent slower depolarization was not different in sham-control versus epileptic animals [Fig. 1L; first-order dendrites $n = 42$ and 47, second-order dendrites $n = 16$ and 29, in sham-control and epileptic, respectively, area under the curve of slow depolarization two-way ANOVA main effect, sham-control versus epileptic: $F(1,130) = 3.51$, $P = 0.063$; first-order versus second-order: $F(1,130) = 1.83$, $P = 0.18$; interaction: $F(1,130) = 0.17$]. These results collectively show a dramatically augmented excitability of proximal, first-order dendrites in epileptic animals, reflected in the prevalence and properties of dendritic spikes.

Reduced synchrony requirement for dendritic spike generation

Synchronous stimulation is required for generation of dendritic spikes in normal pyramidal neurons, and is thought to be critical to detect the coincident activity of specific presynaptic ensembles.[2] Therefore, we tested how dendritic spike generation depends on input synchrony by varying the inter-spine stimulation interval in control and epileptic animals (representative examples in Fig. 2A, sham-control in black, epileptic in red). Epileptic animals exhibited a remarkable loss of their capability to selectively respond to synchronous inputs via generation of dendritic spikes. While sham-control animals exhibited a steep decrease in dendritic spike generation when stimulation was less synchronous, epileptic animals continued to generate dendritic spikes even with very asynchronous stimulations (Fig. 2B; $n = 12$ and 11 in sham-control versus epileptic mice, Fisher's exact test, $P < 0.001$ indicated with asterisks, see figure legend).

Correspondingly, the maximal rate of rise of the fast phase of dendritic spikes (d*V*/d*t*) also showed a much less pronounced reduction with less synchronous stimulation in epileptic animals [Fig. 2C; two-way repeated-measures ANOVA main effects, sham-control versus epileptic: $F(1,21) = 32.34$, $P < 0.0001$; inter-spine time: $F(4,84) = 22.59$, $P < 0.0001$; interaction: $F(4,84) = 9.87$, $P < 0.0001$; Bonferroni's post-tests indicated with asterisks, $P < 0.003$, individual *P*-values see legend]. Intriguingly, in some cases, dendritic branches in epileptic animals were capable of generating multiple sequential spikes ($n = 2$ of 11 branches; example in Fig. 2A, arrow).

Reduced dendritic spike inactivation in chronic epilepsy

Sparse dendritic spiking is supported by inactivation of dendritic spike generation by prior activity, a phenomenon that relies on inactivation of dendritic sodium channels. In control animals, dendritic spike inactivation was observed similar to published data,[26] as indicated by a progressive reduction of dendritic spike d*V*/d*t* until dendritic spike failure (black traces in Fig. 3A; quantification in Fig. 3B and C). In epileptic animals, this reduction in dendritic spike d*V*/d*t* as well as inactivation of spike generation was significantly less pronounced (Fig. 3A–C, statistical results see figure legend).

Thus, collectively, the results show that dendritic spike generation is strongly enhanced, and that multiple mechanisms that underlie sparse generation of dendritic spikes in normal animals are severely degraded in epilepsy.

Involvement of Na$_v$ channels in augmented dendritic integration

The increased incidence of dendritic spikes, as well as the increased rate of rise of the fast phase of the dendritic spikes suggests upregulation of Na$^+$ channels as a potential mechanism, and raises the possibility that anticonvulsants targeting Na$^+$ channels might affect this phenomenon. We first tested if the Na$^+$ channel blocker and anticonvulsant S-Lic (300 µM) affect aberrant dendritic spikes (Fig. 4A–K). S-Lic did not affect the properties of uEPSPs (Supplementary Fig. 5A–D). Surprisingly, application of S-Lic also did not alter the threshold for eliciting dendritic spikes in either control or epileptic animals [Fig. 4C and G; spike thresholds indicated with dashed lines, quantification in Fig. 4D and H, $n = 8$ and 5 in sham-control versus epileptic; two-way repeated-measures ANOVA main effect, sham-control versus epileptic: $F(1,11) = 5.82$, $P = 0.044$; ACSF versus S-Lic: $F(1,11) = 0.86$, $P = 0.37$; interaction: $F(1,11) = 0.47$, $P = 0.51$, Bonferroni's post-test n.s.]. Likewise, S-Lic did not affect the rate of rise of dendritic spikes in epileptic animals [Fig. 4B and F; two-way repeated-measures ANOVA main effect, sham-control versus epileptic: $F(1,11) = 27.76$, $P = 0.0003$; ACSF

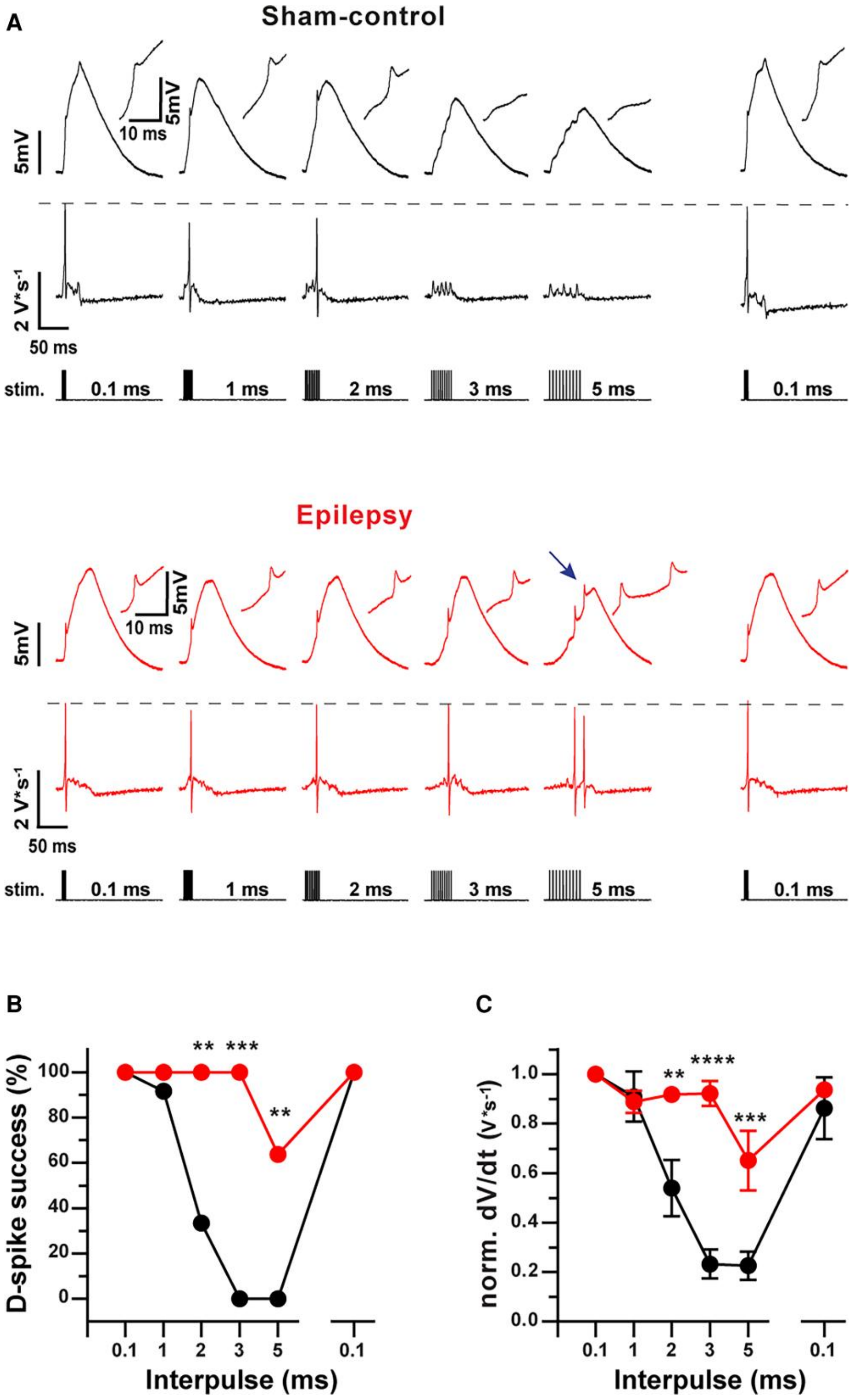

Figure 2 Degraded synchrony requirement in epileptic mice. (**A**) Representative example traces showing input synchrony dependence of dendritic spikes in CA1 neurons from sham-control and epileptic mice. Changing the inter-spine stimulation interval (*bottom rows* in Sham-control and Epileptic) systematically affects dendritic spike generation in control and epileptic animals. Upper rows show somatic voltage response, middle rows show first derivation of the voltage trace (dV/dt). Note that the rightmost response is again elicited with a 0.1 ms inter-spine stimulation interval, applied following the longer intervals. (**B** and **C**) Rate of spike occurrence in percent of uncaging stimulations (D-spike success) and dendritic-spike strength expressed as the maximal rate of rise (dV/dt) of the fast phase of the dendritic spike. Asterisks in **B** correspond to significance in Fisher's exact test, with the following P-values: 2 ms $P = 0.0013$; 3 ms $P < 0.0001$; 5 ms $P = 0.0013$. Asterisks in **C** correspond to significances in Bonferroni's post-tests for inter-spine stimulation intervals 2 ms $P = 0.0013$; 3 ms $P < 0.0001$; 5 ms $P = 0.0003$.

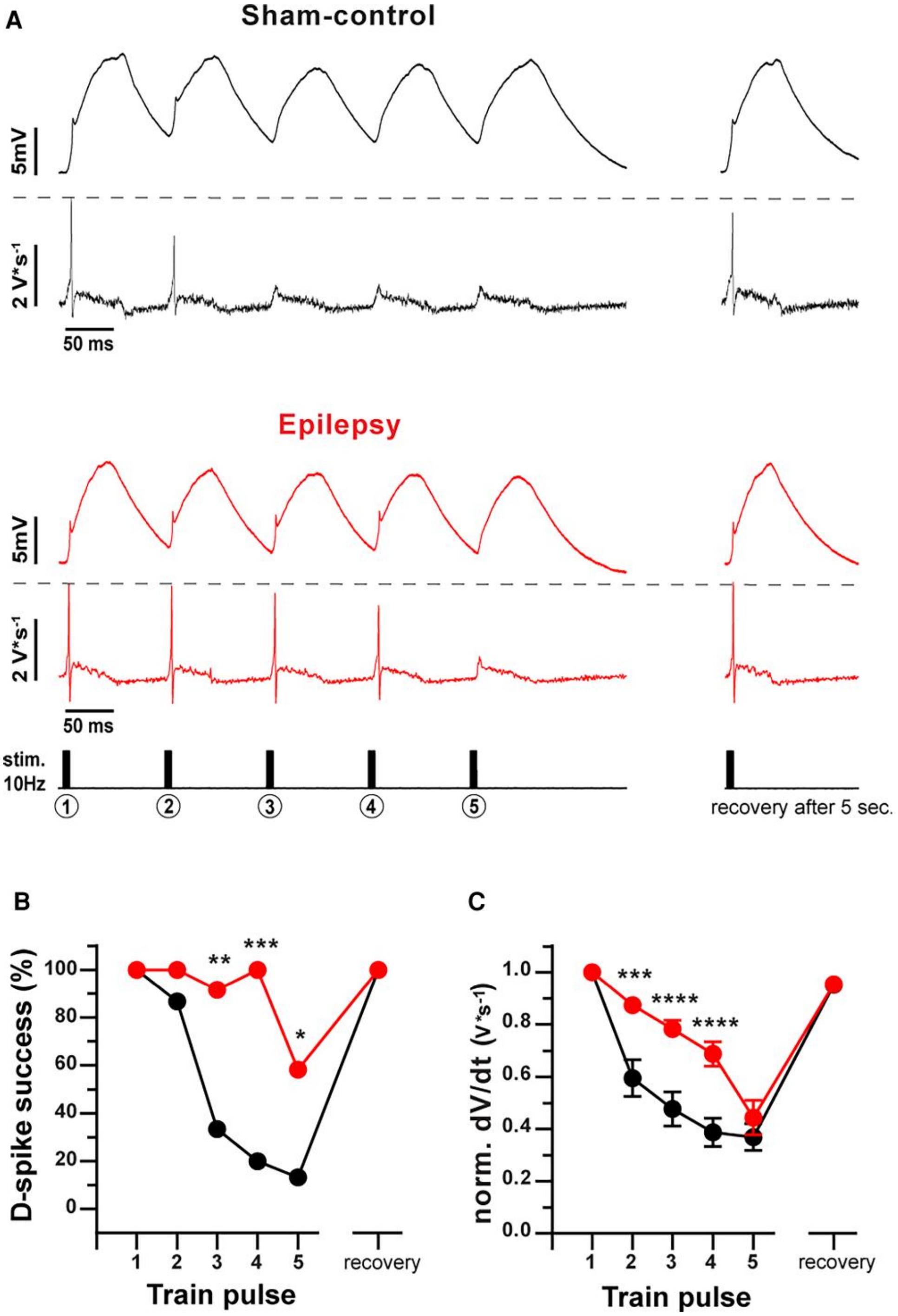

Figure 3 Degraded dendritic spike inactivation in chronic epilepsy. (**A**) Representative somatic voltage recordings from a sham-control (black) and epileptic (red) mouse (*upper trace*) with the corresponding first derivation of the voltage trace (dV/dt) shown below. Dendritic spikes were repetitively elicited with synchronous stimulation at 10 Hz (*lowermost trace*). (**B**) The fraction of stimuli successfully generating dendritic spikes strongly decreased with repetitive stimulation (n as in **C**, asterisks indicate Fisher's exact test, third stimulation $P = 0.001$, fourth stimulation $P = 0.0001$, fifth stimulation $P = 0.037$). (**C**) Spike strength (dV/dt) also decreases steeply with repetitive stimulation in control (black) but not in epileptic animals (red). Sham-control $n = 15$, epileptic mice $n = 12$. Two-way repeated-measures ANOVA revealed main effects, sham-control versus epileptic: $F(1,25) = 12.51$, $P < 0.0016$; repetitive stimulation: $F(4,100) = 80.57$, $P < 0.0001$; interaction: $F(4,84) = 8.30$, $P < 0.0001$); asterisks indicate Bonferroni's post-test, dV/dt for second stimulation $P = 0.0006$, third stimulation $P = 0.0001$, fourth stimulation $P = 0.0002$.

versus S-Lic: $F(1,11) = 1.30$, $P = 0.28$; interaction: $F(1,11) = 2.51$, $P = 0.14$, Bonferroni's post-test n.s.]. In contrast to the lack of effect on dendritic spikes, S-Lic significantly inhibited somatic action potential generation [Fig. 4I–K and Supplementary Fig. 5E–P; for statistics see Supplementary Fig. 6 legend] as described previously (see e.g. Doeser *et al.*[15] and Schmidt *et al.*[27]).

At this concentration, S-Lic has been shown to have strong preferential effects on the availability of $Na_v1.2$ and 1.6 channels, with

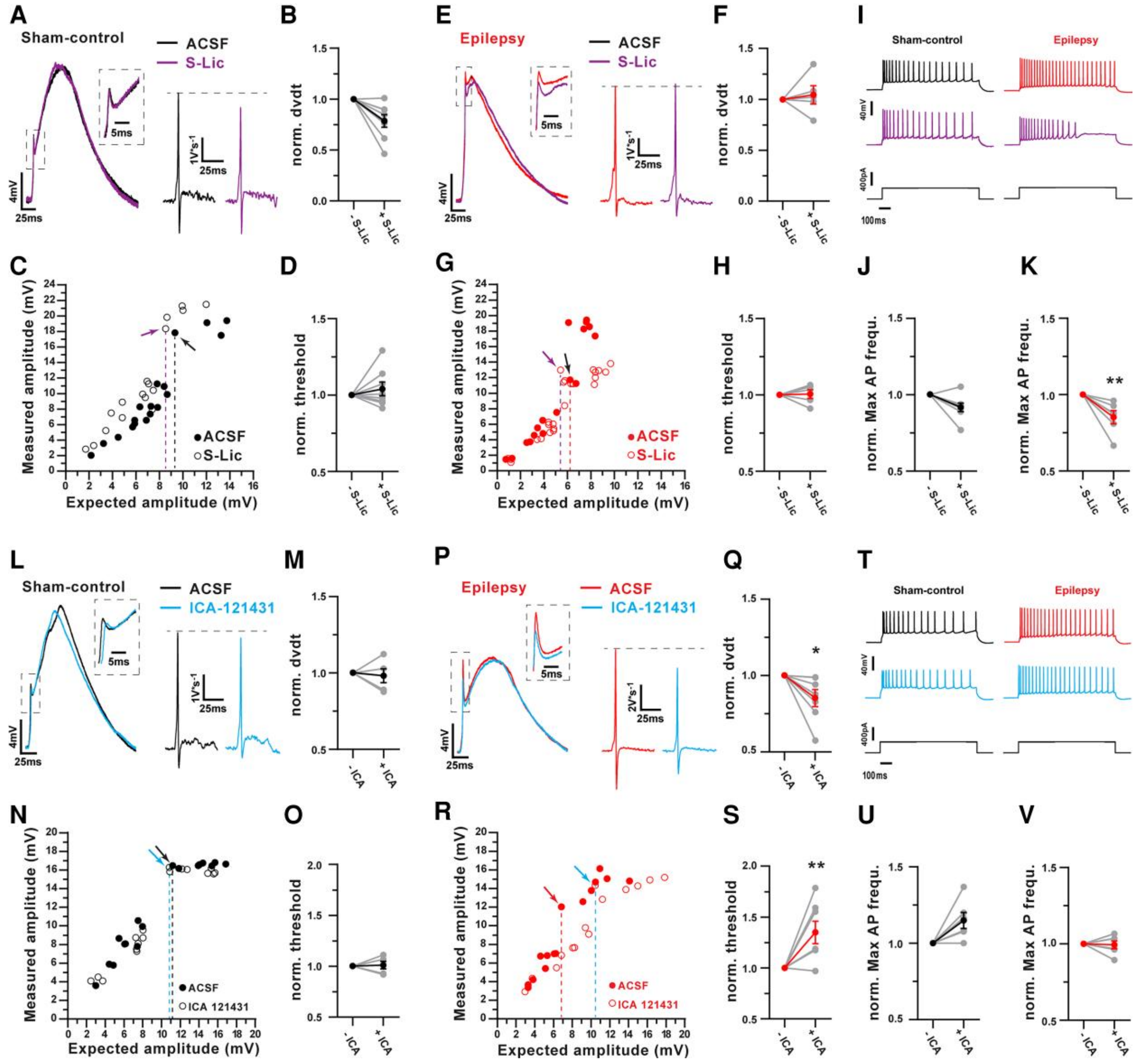

Figure 4 The Na$_v$1.3/1.1 selective blocker ICA-121431, but not the Na$_v$1.2/1.6 Na$^+$ channel blocker S-Lic reverses enhanced dendritic excitability. (**A** and **E**) Representative examples of the effects of the Na$_v$1.2/1.6 Na$^+$ channel blocker S-Lic (300 µM) on dendritic spikes (*insets* show magnification of the fast phase of the dendritic spike), and on the first derivation of the voltage trace (dV/dt) in sham-control (**A**) and epileptic (**E**) animals. (**B** and **F**) Effects of S-Lic on the maximal rate of rise of the dendritic spike in sham-control (**B**) and epileptic mice (**F**). (**C** and **G**) Representative examples of effects on the dendritic spike threshold in sham-control and epileptic mice (arrows indicate occurrence of dendritic spikes and dashed lines indicate thresholds). (**D** and **H**) Quantification showing the lack of significant effects on the dendritic spike threshold in sham-control (**D**) and epileptic mice (**H**) with S-Lic application. Two-way ANOVA revealed no significant effects of S-Lic on the rate of rise or threshold of dendritic spikes in control (**B** and **D**) and epileptic (**F** and **H**) animals. (**I**–**K**) Effects of S-Lic on somatic action potential generation. Representative examples of repetitive firing evoked by somatic current injection in sham-control and epileptic mice in ACSF and in the presence of S-Lic (violet, **I**). Effects of S-Lic on firing induced by current injection at which firing frequency was maximal under ACSF conditions, control and epileptic animals (**I** and **K**, respectively). Asterisks indicate Bonferroni's post-test $P = 0.0034$. (**L**–**S**) Effects of the Na$_v$1.3/1.1 Na$^+$ channel blocker ICA-121431 (100 nM) in sham-control (**L**–**O**) and epileptic animals (**P**–**S**), depicted in the same manner as in panels (**A**–**H**). Asterisks indicate Bonferroni's post-test, $P = 0.023$ (**Q**) and $P = 0.0050$ (**S**). (**T**–**V**) Lack of effects of ICA-121431 on somatic action potential generation. Representative examples of repetitive firing evoked by somatic current injection in sham-control and epileptic mice in ACSF and in the presence of ICA-121431 (blue, **T**). Lack of effects of ICA-121431 on the maximal firing frequency of CA1 neurons (**U** and **V**).

very little effect on Na$_v$1.3 or 1.1 channels at resting membrane voltages.[17] This raises the possibility that one of these latter channel types underlies increased dendritic spiking, even if Na$_v$1.3 or 1.1 channels are normally not expressed at high levels in adult pyramidal neurons. To test this idea, we took advantage of the selective Na$_v$1.3/1.1 blocker ICA-121431[18] at 100 nM, a concentration which blocks Na$_v$1.3 and Na$_v$1.1 (Fig. 4L–S). In these experiments, we specifically selected uncaging sites on dendrites that exhibited robust and noticeable dendritic spikes to assess if ICA-121431 blocked them. Due to this bias, differences in spike properties between sham-control and epileptic animals are not present in this experiment.

ICA-121431 did not alter the properties of uncaging-evoked single-spine EPSPs (Supplementary Fig. 5A–D). However, in epileptic, but not in sham-control animals, ICA-121431 (100 nM) significantly increased the dendritic spike threshold [Fig. 4N and R, spike thresholds indicated with dashed lines, Fig. 4O and S; in summary, $n = 5$ and 7 in sham-control versus

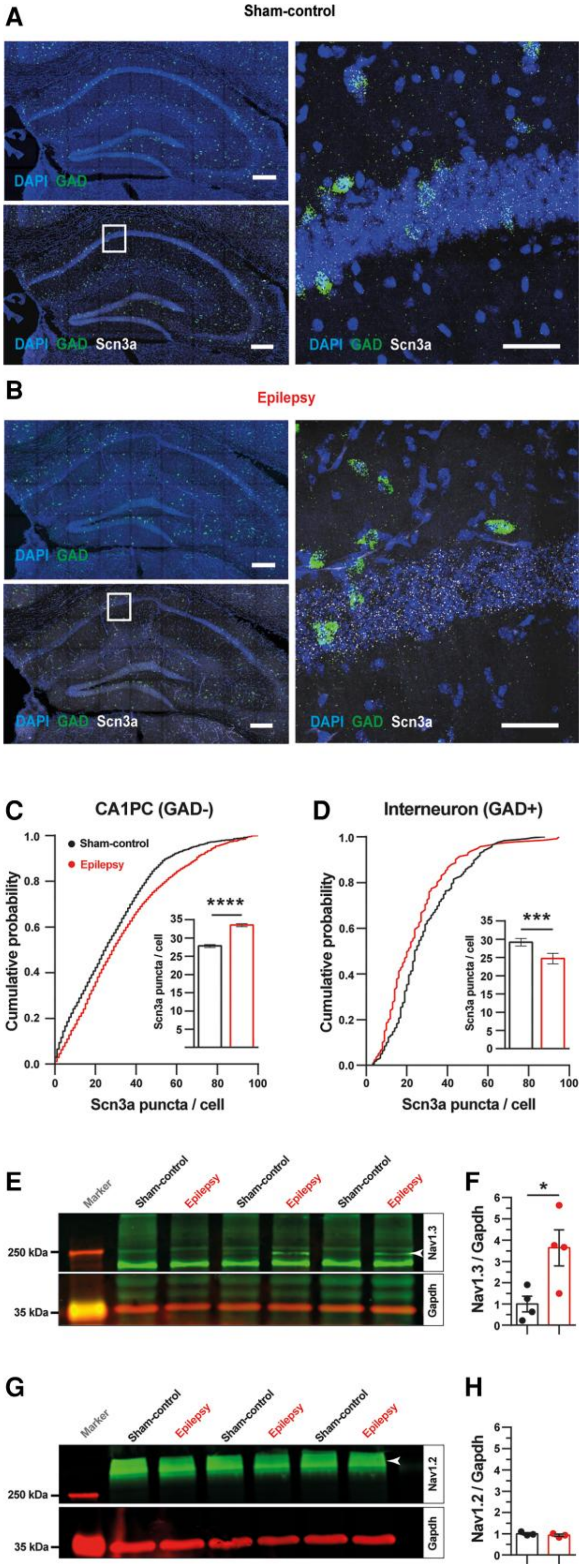

Figure 5 ***Scn3a* expression is increased at the mRNA and protein level in the hippocampal CA1 region of epileptic mice.** (**A**–**D**) Multiplex fluorescent mRNA *in-situ* hybridization for *Scn3a* in hippocampal CA1 region. (**A** and **B**) Representative fluorescent images showing labelling of nuclei with DAPI (blue), labelling of GABAergic neurons (GAD) with a probe for *Gad1/2* mRNA (green) and of *Scn3a* mRNA (red) in hippocampal

(Continued)

Figure 5 Continued
slices from sham-control and epileptic animals, scale bar 500 µm. Close up (*right*) of the boxed areas, scale bar = 100 µm. (**C**) Cumulative distribution of *Scn3a* punctae per nucleus colocalized excitatory pyramidal cells (excluding GAD-labelled putative interneurons). The amount of punctae was significantly higher in epileptic animals (2979 cells in six animals and 3669 cells in five animals, for sham-control and epileptic mice, respectively; asterisks indicate Kolmogorov–Smirnov two-tailed test $P < 0.0001$). (**D**) Cumulative distribution of *Scn3a* punctae per nucleus colocalized in GAD+ interneurons. The amount of punctae was significantly lower in epileptic animals (253 cells in five animals and 141 cells in five animals, for sham-control and epileptic mice, respectively; asterisks indicate Kolmogorov–Smirnov two-tailed test $P < 0.001$). (**E**–**H**) Western blots for $Na_v1.3$ and $Na_v1.2$ in hippocampal CA1 region. (**E**) Representative Western blots of $Na_v1.3$ (indicated with arrrowhead) and the housekeeping protein GAPDH, used as loading control in sham-control and epileptic mice. (**F**) Quantitative analysis of the $Na_v1.2$ protein obtained by band intensity analysis from **E** (normalized $Na_v1.2$/GAPDH ratio of 1.0 ± 0.36 in sham-control $n = 4$ and 3.64 ± 0.85 in epileptic mice $n = 4$; unpaired Student's *t*-test $P = 0.029$; data represent mean ± SEM). (**G**) Representative Western blots of $Na_v1.2$ (indicated with arrrowhead) and the housekeeping protein GAPDH, used as loading control in sham-control and epileptic mice. (**H**) Quantitative analysis of the $Na_v1.2$ protein obtained by band intensity analysis from **G** (normalized $Na_v1.2$/GAPDH ratio of 1.0 ± 0.05 in sham-control $n = 3$ and 0.93 ± 0.052 in epileptic mice $n = 3$; unpaired Student's *t*-test $P = 0.38$).

epileptic, two-way repeated-measures ANOVA main effect, sham-control versus epileptic: $F(1,10) = 0.008$, $P = 0.93$; ACSF versus ICA-121431: $F(1,10) = 6.24$, $P = 0.032$; interaction: $F(1,10) = 7.10$, $P = 0.024$; Bonferroni's post-test epileptic ACSF versus ICA-121431 $P = 0.0050$]. Likewise, ICA-121431 decreased the rate of rise of dendritic spikes only in epileptic animals [see insets for dV/dt traces in Fig. 4L and P and summary in Fig. 4M and Q; two-way repeated-measures ANOVA main effect, sham-control versus epileptic: $F(1,10) = 0.050$, $P = 0.82$; ACSF versus ICA-121431: $F(1,10) = 5.36$, $P = 0.043$; interaction: $F(1,10) = 2.50$, $P = 0.14$; Bonferroni's post-test epileptic ACSF versus ICA-121431 $P = 0.025$]. The NMDA-receptor-driven slow phase of the dendritic spike was unaffected by ICA-121431 (two-way repeated-measures ANOVA, n.s.).

We then tested if, in addition to the significant effects on dendritic integration in epileptic animals, blocking $Na_v1.3/1.1$ channels also affects the generation of somatic action potentials. Surprisingly, ICA-121431 had no effects on action potential generation or repetitive firing induced by somatic current injection in either control or epileptic animals [Fig. 4T–V, Supplementary Fig. 5E–P and Supplementary Table 2; $n = 6$ in both groups, two-way repeated-measures ANOVA main effect, sham-control versus epileptic: $F(1,10) = 11.66$, $P = 0.0066$; ACSF versus ICA-121431: $F(1,10) = 1.67$, $P = 0.23$; interaction: $F(1,10) = 2.28$, $P = 0.16$, Bonferroni's post-tests, n.s.].

This suggests that the $Na_v1.3/1.1$ blocker ICA-121431 selectively affects dendritic spikes rather than somatic firing, while S-Lic does the converse, and raises the possibility that subtype selective Na^+ channel antagonists may be useful in selectively dampening dendritic hyperexcitability in epilepsy.

$Na_v1.3$ channels have been previously described to exhibit increased expression in acquired experimental epilepsy, while $Na_v1.1$ channels are downregulated.[28] To confirm the upregulation of $Na_v1.3$ in our model, we investigated *Scn3a* expression at the mRNA level at single-cell resolution. To this end, we used multiplex RNA *in-situ* hybridization (RNAscope, see 'Materials and methods' section; Fig. 5A and B). Low levels of *Scn3a* mRNA puncta were present in pyramidal neurons in the adult hippocampus (Fig. 5A). However, we found a significant upregulation of *Scn3a* expression in pyramidal neurons from epileptic animals (Kolmogorov–Smirnov test $P < 0.0001$ sham-control $n = 5$, epileptic mice $n = 6$; Fig. 5C). In contrast, GAD-expressing interneurons showed downregulation of *Scn3a* compared with sham-control animals (sham-control $n = 5$ epileptic mice $n = 5$, Kolmogorov–Smirnov two-tailed test, $P < 0.001$; Fig. 5D).

We then assessed $Na_v1.3$ protein level in the hippocampus using Western blot analyses. Consistent with the *Scn3a* mRNA puncta the protein level of $Na_v1.3$ in CA1 subregion was low in sham animals and up to four times higher in tissue from epileptic animals (sham-control $n = 4$ and epileptic mice $n = 4$, Student's *t*-test, $P = 0.02$; Fig. 5E and F). This is in contrast to $Na_v1.2$ protein, which was not significantly different between sham-control and epileptic animals (sham-control $n = 3$ and epileptic mice $n = 3$, Student's *t*-test two-tailed, $P = 0.38$; Fig. 5G and H).

ICA-121431 normalizes aberrant place-related firing of CA1 neurons *in vivo*

These data point towards a substantial decrease in specificity of dendritic spikes and degraded input feature detection. Because dendritic spikes are thought to play an important role in shaping place field properties of CA1 neurons,[4] we hypothesized that aberrant dendritic spikes might be associated with degraded place coding in CA1 neurons *in vivo*. We therefore examined the activity of CA1 neurons using two-photon Ca^{2+} imaging in head-fixed sham-control and epileptic *Thy1-GCaMP6s* mice running on a linear track equipped with spatial cues (Fig. 6A–D and Supplementary Fig. 6A–D). As described previously, the activity of CA1 neurons was higher during locomotion in both the sham-control and epileptic mice. Additionally, we observed a markedly increased activity of CA1 neurons in epileptic animals compared to sham control animals, both during immobility and locomotion (Supplementary Fig. 6E–G; $n = 1022$ CA1 neurons in five sham-control mice and 1697 CA1 neurons in six epileptic mice; for statistics see figure legend).

CA1 neurons that exhibited significant place-related activity[23] were found in both sham-control and epileptic mice (examples of representative neurons in Fig. 6E, spiral plots show place coding, rightmost distributions show tests versus shuffled distributions for each cell). In both sham-control and epileptic mice, place-related firing fields tiled the extent of the linear track (Fig. 6F, upper panels all significantly place-coding CA1 neurons from a representative sham-control and epileptic mouse, respectively; Fig. 6G, upper panels for data from all sham-control and epileptic mice). It was apparent from visual inspection of these data that place-related firing of significantly place-coding cells appeared to be less specific in epileptic animals, consistent with published work demonstrating degraded place coding in epileptic animals.[29–32] We quantified the precision of spatial coding using a spatial tuning vector measure[23,33] (see also place vectors in spiral plots in Fig. 6E), where higher place coding specificity corresponds to greater vector lengths. Indeed, we found the distribution of place vector lengths was significantly shifted to shorter values in epileptic mice, implying degraded place coding (Fig. 6H, cf. left and right panels). This difference was stable over multiple sessions of imaging (Fig. 6I), indicating decreased specificity of place coding in epileptic animals.

We next examined if ICA-121431, which normalized the properties of dendritic spikes *in vitro*, also improves place coding in epileptic mice. Indeed, in the presence of ICA-121431, the precision of place coding assessed by spatial tuning vector lengths significantly increased in epileptic but not in sham-control mice (cumulative distributions of vector lengths for all cells in Fig. 6H). Correspondingly, ICA-121431 also caused an increase of the average vector lengths calculated per mouse in epileptic, but not in sham-control mice [Fig. 6J; $n = 6$ and 5 mice, respectively, repeated-measures two-way ANOVA main effects, sham-control versus epileptic: $F(1,9) = 6.29$, $P = 0.033$; baseline versus ICA-121431 treatment: $F(1,9) = 3.92$, $P = 0.079$; interaction: $F(1,9) = 5.64$, $P = 0.042$; Bonferroni's post-test sham-control versus epileptic $P = 0.0095$, epileptic mice before ICA-121431 treatment versus ICA-121431 treated epileptic mice $P = 0.0207$]. When we computed the effects on average vector lengths in each animal, the effect of ICA-121431 was significantly larger in epileptic mice, as expected (Fig. 6K; Mann–Whitney U-test, $P = 0.030$). These experiments suggest that reversing dendritic hyperexcitability with ICA-121431 *in vivo* significantly reverses degraded place coding in epilepsy.

It is known that place coding can be disrupted by interictal synchronous activity.[32,34] To elucidate if effects of ICA-121431 on place-related firing in epileptic animals could also be due to an inhibition of aberrant synchronous activity, we tested the effects of this compound on population activity in the CA1 region. We found aberrant synchronized activity in epileptic mice, but never in sham-control mice (an example in an epileptic mouse is shown in Supplementary Fig. 7A–C). In epileptic mice, we examined the effects of ICA-121431 on short events most likely corresponding to interictal spikes[35] and longer duration events (1–5 s and >5 s). In all three of these categories, the average number and duration of events was not affected by ICA-121431 (Supplementary Fig. 7D–O; see Supplementary material for analysis methods and Supplementary Fig. 7 legend for statistics).

ICA-121431 normalizes hippocampal-dependent memory in epileptic mice

We next asked if reversing aberrant dendritic excitability with ICA-121431 *in vivo* restores performance in a hippocampus-dependent spatial memory task. We selected a task in which rodents learn the spatial arrangement of two objects. In a subsequent session, one of the objects is displaced (OLM test), and the increased exploration of the displaced object is measured. In subsequent experiments, one of the objects is exchanged for a novel object (NOR test). After habituation for 3 days, treatment was started with either vehicle or ICA-121431 during the fourth habituation day (Fig. 7A and B). Subsequent sessions for the OLM test were carried out either in the presence of vehicle or ICA-121431. During acquisition of the object position for the OLM test, mice did not discriminate the two objects (Fig. 7C, upper panels; Fig. 7E, two-way ANOVA, n.s.). In the OLM trial with a displaced object, vehicle-treated sham-control mice discriminated the displaced object, while vehicle-treated epileptic animals did not (Fig. 7C, lower panels, $n = 17$ and 15, respectively; filled bars in Fig. 7F). Importantly, administration of ICA-121431 by gavage (see 'Materials and methods' section) recovered memory performance to control levels in epileptic animals (Fig. 7D, lower panels, $n = 7$ and 8 for sham-control and epileptic animals, respectively; empty bars in Fig. 7F). Two-way ANOVA revealed a main effect of vehicle versus ICA-121431 treatment [vehicle versus ICA-121431: $F(1,43) = 5.95$, $P = 0.019$; sham-control versus epileptic: $F(1,43) = 1.17$, $P = 0.29$; interaction: $F(1,43) = 3.91$, $P = 0.054$ Bonferroni's post-tests indicated with asterisks].

In contrast to the OLM trial, NOR was not impaired in epileptic animals (Fig. 7G and J), consistent with previous reports.[24] ICA-121431 treatment did not alter performance in the NOR trial in either sham-control or epileptic mice (Fig. 7I and J; *n* as for OLM trials; statistics, Fig. 7 legend).

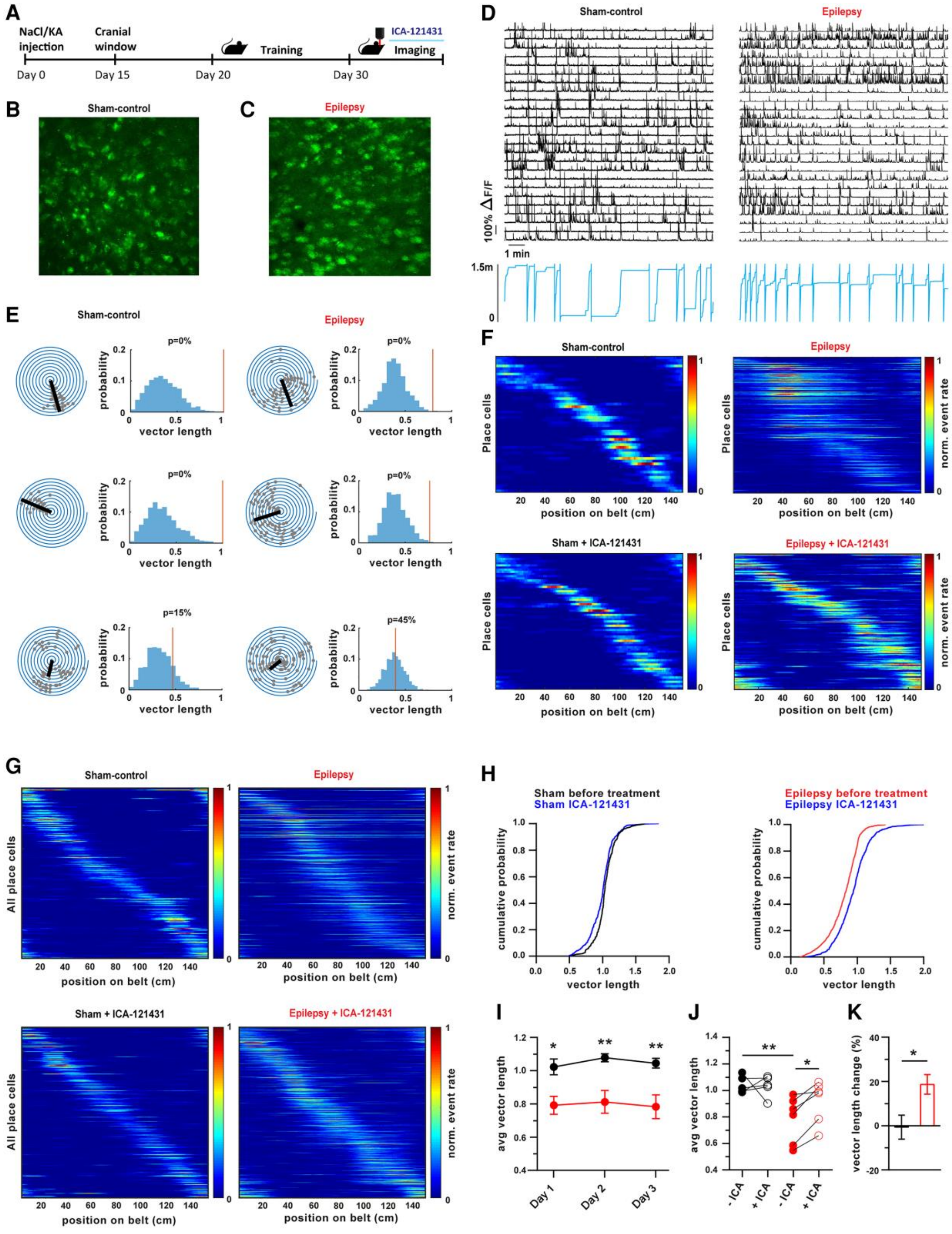

Figure 6 ICA-121431 normalizes place-related firing of CA1 neurons from epileptic mice *in vivo*. (**A**) Experimental protocol used to examine the activity of CA1 neurons using two-photon Ca^{2+} imaging in *Thy1-GCaMP6s* mice running on a linear track. (**B** and **C**) Representative fields of view obtained for *in vivo* imaging. (**D**) Representative examples of activity in a subset of the CA1 neurons from the fields of view shown in **B** and **C**. *Upper traces* indicate ΔF/F traces from a subset of CA1 neurons, *lower traces* (blue) indicate position of the mouse. (**E**) Analysis of place coding. Spiral plots for three representative CA1 neurons in a sham-control mouse (*left*) and an epileptic mouse (*right*). One 360° pass around the spiral plot corresponds to a complete transition on the 150 cm circular linear treadmill. Grey circles indicate event onsets in the CA1 neuron. Computed place vectors indicated by black straight lines. Distributions on the right show tests versus shuffled distributions for each cell (see 'Materials and methods' section for details). The red vertical lines indicate the vector length of the CA1 neuron, shuffled distributions shown in blue. (**F**) All significantly place-coding CA1 neurons from a representative sham-control (*left*) and epileptic mouse (*right*). *Lower panels* show the same mice following treatment with ICA-121431. (**G**) Panels

(Continued)

We next investigated if ICA-121431 affects performance in a spatial working memory task, spontaneous alternation in the Y-maze. In this task, animals freely explore a three-arm maze. The extent to which animals sequentially explore three different arms is quantified (alternation score), with higher alternation scores indicating a higher level of efficient exploration requiring spatial working memory (Fig. 7K–M). ANOVA revealed main effects on the alternation score of kainate treatment [sham-control versus epileptic: $F(1,44) = 7.36$, $P = 0.0095$], but the effects of ICA-121431 treatment did not reach statistical significance [$F(1,44) = 2.86$, $P = 0.098$; interaction: $F(1,44) = 0.82$, $P = 0.59$; Fig. 7M, Bonferroni's post-tests indicated with asterisks]. Thus, the effects of ICA-121431 seem to be most prevalent for spatial tasks that require hippocampal-dependent memory consolidation.

Discussion

In this paper, we describe a Na^+ channel-dependent mechanism underlying a prominent change in dendritic supralinear integration in epilepsy that degrades place coding *in vivo* and causes deficits in spatial memory.

Dendritic spikes are a cornerstone of dendritic integration that enable neurons to generate precise action potential outputs to clustered inputs deriving from specific populations of presynaptic input neurons. They are therefore important in mediating sharply tuned neuronal responses to features of input neurons.[1,36] We show that the properties of dendritic spike generation are markedly altered in CA1 pyramidal cells in chronic epilepsy. Specifically, the fraction of dendritic branches that can give rise to dendritic spikes is almost doubled in epileptic animals. In addition, in those dendrites that generate dendritic spikes, virtually all properties that confer input-specificity to dendritic spikes are degraded. First, even very asynchronous stimulations can cause dendritic spikes in epileptic animals. Second, the threshold for eliciting dendritic spikes is significantly lowered in epileptic animals. Third, mechanisms that usually attenuate dendritic spikes upon prior occurrence of somatic or dendritic spikes[26] are much less effective in epileptic animals. Fourth, dendritic spikes rise at an enhanced rate in first-order dendrites from epileptic animals. Because dendritic spikes with a high rate of rise (also termed 'strong' spikes) are much less affected by concurrently evoked inhibition,[37] this predicts decreased inhibitory control of dendritic spikes in epileptic animals. The changes in dendritic integrative properties were primarily present in first-order and not second-order dendrites. This is reminiscent of the changes observed following environmental enrichment, in which dendritic spikes in first-order branches are selectively strengthened.[38] In this paradigm, strengthening of proximal branches led to an enhanced propagation of distally evoked dendritic spikes into first-order dendrites.[38] Importantly, epilepsy-related changes in dendritic integration are observed in CA1, but not in other hippocampal subregions such as the dentate gyrus.[39]

Together, these findings suggest that input feature detection of CA1 neurons is degraded in epileptic animals, and predict much less selective task- or stimulus-specific response properties. We have used place coding as a model to test this idea. Place cells within the CA1 fire specifically when a rat occupies a particular location in the environment.[40] Dendritic spiking has been proposed to be essential in driving formation of place-related firing in CA1 neurons,[4,41,42] and computational studies have suggested that sharp spatial tuning of place cell responses is supported by dendritic spikes.[43] Indeed, we have found significant broadening of place representations in epileptic animals, consistent with previous studies in different models of epilepsy.[29–31,44] This idea is also in line with computational studies suggesting that changes causing an increase in dendritic spike generation degrade place tuning of pyramidal neurons.[43,45] Importantly, the absence of dendritic spikes also degrades spatial tuning, suggesting that the prevalence and properties of dendritic spikes have to be carefully tuned for optimal place coding.[45]

Our data suggest an upregulation of dendritic Na^+ channels, consistent with a somato-dendritic upregulation of persistent Na^+ channels described in a different model of experimental TLE.[10] Our pharmacological data using antagonists with preferential activity on $Na_v1.2/1.6$ (S-Lic) versus $Na_v1.3/1.1$ (ICA-121431) do not allow us to unequivocally pinpoint the identity of the channel mediating enhanced excitability of first-order CA1 dendrites. However, several lines of evidence suggest that $Na_v1.3$ upregulation is the more probable underlying mechanism. First, we and others have shown that upregulation of $Na_v1.3$ occurs in models of acquired and genetic epilepsy,[28, 46] while $Na_v1.1$. expression is reduced.[28] Second, $Na_v1.3$ channels exhibit rapid repriming and recovery from inactivation, as well as particularly slow closed-state inactivation, properties that are well suited to explain repetitive generation of dendritic spikes and loss of dendritic spike inactivation.[47]

$Na_v1.2$ has also been implicated in dendritic excitability, with loss of $Na_v1.2$ channels decreasing action potential backpropagation into pyramidal cell dendrites.[48] Of note, this study has mainly focused on the main apical dendritic trunk, and not the first- and second-order apical oblique dendrites that generate dendritic spikes and that we studied in our experiments. Which sodium channel subtypes drive dendritic spikes in these dendrites in control animals is still unclear. Irrespective of this question, our data show that $Na_v1.2$ channel protein is unaltered in epileptic mice, consistent with the idea that an additional expression of $Na_v1.3$ is the major driver in increased dendritic excitability.

Although the convergent *in vitro* and *in vivo* data point to a role of dendritic Na_v channels, additional changes also influence processing of CA1 neurons during navigation. Inhibition is strongly altered in chronic epilepsy, with changes in the amount and timing of inhibition delivered by inhibitory circuits,[49–51] a factor that may also contribute to altered place coding. However, it has been argued that the development of interneuron loss and seizures occurs long before instability of place representations is observed,[31] suggesting that interneuron loss alone cannot account for this

Figure 6 Continued
show all CA1 neurons in the two experimental groups (sham-control and epileptic), both before and during application of ICA-121431. (**H**) Cumulative distributions of place vector lengths for sham-control (*left*) and epileptic mice (*right*). Blue curves indicate cumulative distribution of vector lengths after application of ICA-121431. (**I**) Differences between average vector lengths in sham-control (black) and epileptic animals (red) were stable over imaging sessions on three consecutive days. Two-way ANOVA main effect, sham-control versus epileptic: $F(1,27) = 31.12$, $P < 0.0001$; subsequent days: $F(2,27) = 0.2623$, $P = 0.7727$; interaction: $F(2,27) = 0.05973$, $P = 0.9421$; asterisks indicate Bonferroni's post-test, Day 1 $P = 0.02$, Day 2 $P = 0.0066$ and Day 3 $P = 0.0074$. (**J**) Average vector lengths calculated per mouse in sham-control (black) and epileptic mice (red). Asterisks indicate Bonferroni's post-tests sham-control versus epileptic $P = 0.0095$, epileptic mice before ICA-121431 treatment versus ICA-121431 treated epileptic mice $P = 0.0207$. (**K**) Percent change in vector length caused by ICA-121431, quantified for each animal and averaged. Asterisk indicates Mann–Whitney U-test, $P = 0.030$.

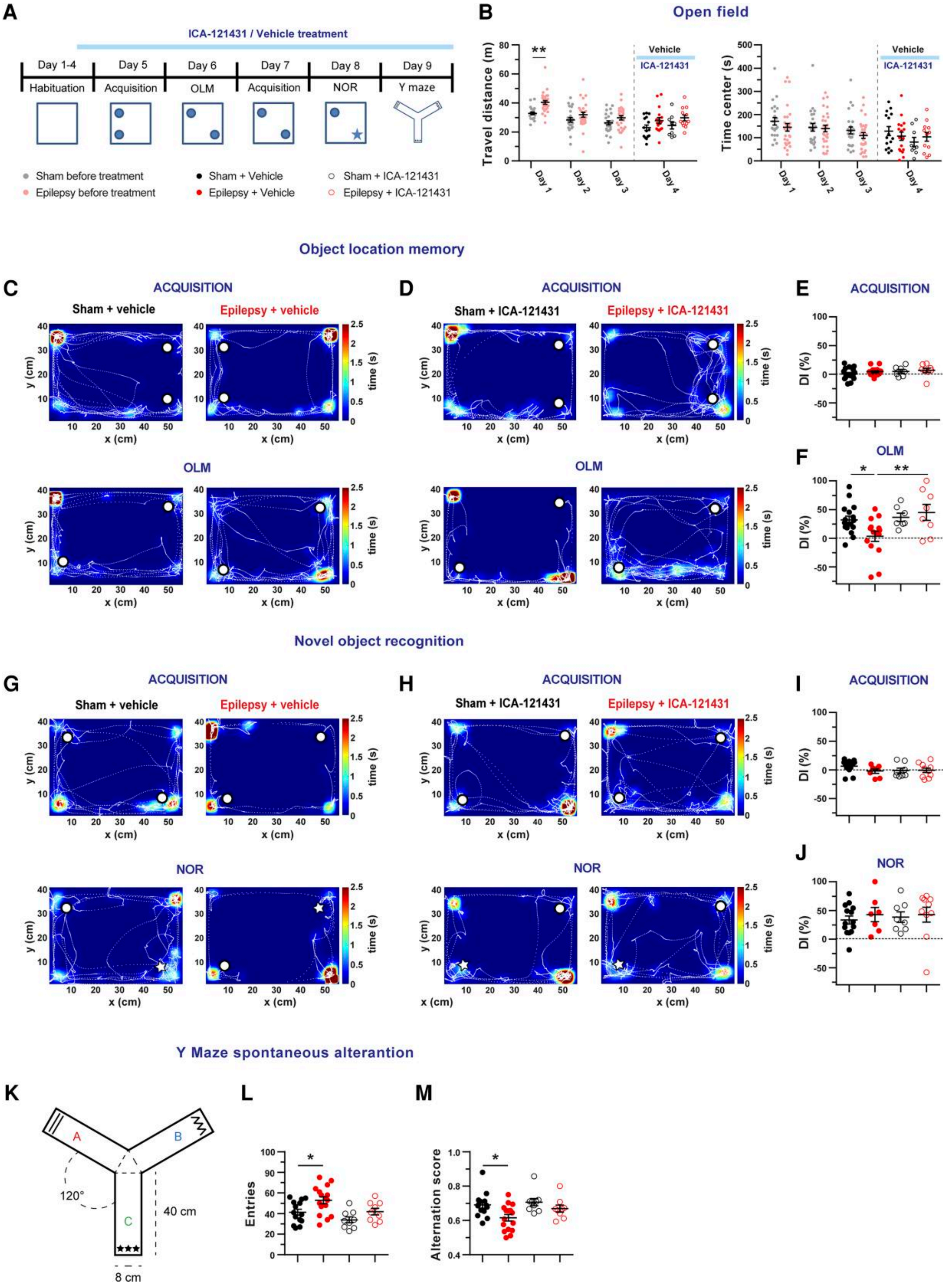

Figure 7 ICA-121431 normalizes hippocampal-dependent memory in epileptic mice. (**A**) Timeline of the behavioural experiments with *in vivo* application of ICA-121431. After habituation to the open field, the OLM, NOR and Y-maze spontaneous alternation tests were performed sequentially. (**B**) Four days of habituation in the open field, with application of either vehicle or ICA-121431 on the fourth day. Animals habituated to the open field on Days 1–3, with progressively less exploration on consecutive days. *Left panel* shows exploration times. Apart from the first day, the exploration times were similar with respect to distance travelled during the session and time spent in the centre of the open field in sham-control versus epileptic groups [$n = 24$ and 29 in sham-control and epileptic mice, two-way ANOVA main effect, sham-control versus epileptic: $F(1,51) = 8.45$, $P = 0.0054$;

(Continued)

Figure 7 Continued
Days 1–3 sessions: $F(2,102) = 39.27$, $P < 0.0001$; interaction: $F(2,102) = 2.14$, $P = 0.12$. Bonferroni's post-test, sham-control versus epileptic Day 1 $P = 0.0015$, sham-control Day 1 versus Day 2 $P = 0.0053$; Day 1 versus Day 3 $P < 0.0001$; Day 2 versus Day 3 $P = 0.62$, travel distance in epileptic mice Day 1 versus Day 2 $P < 0.0001$; Day 1 versus Day 3 $P < 0.0001$; Day 2 versus Day 3 $P = 0.39$]. There was no effect of ICA-121431 application when comparing against the values from Day 3 of habituation, after habituation to the open field (two-way ANOVA, n.s.). *Right panel* shows time spent in the centre, >5 cm away from walls. Two-way ANOVA main effect, sham-control versus epileptic: $F(1,51) = 1.2$, $P = 0.28$; Day 1–3 sessions: $F(2,102) = 7.32$, $P = 0.0011$; interaction: $F(2,102) = 0.59$, $P = 0.56$. Bonferroni's post-test, sham-control Day 1 versus Day 3 $P = 0.02$. Epileptic group Day 1 versus Day 3 $P = 0.030$. (**C**–**F**) Results of the OLM test. (**C** and **D**) Representative examples of session with tracking data in sham-control and epileptic animals with vehicle application (**C**) and ICA-121431 application (**D**), respectively. Occupancy times are colour-coded (for calibration see scale bar). (**E**) The discrimination index (DI) indicating if mice preferentially explore an object during the acquisition session. DI was close to zero, indicating that mice did not discriminate the two objects in any group. (**F**) DI in the OLM session. Vehicle-treated sham-control mice discriminated the displaced object, while vehicle-treated epileptic animals did not (black and red filled bars, respectively). Administration of ICA-121431 by gavage recovered memory performance to control levels in epileptic animals (empty bars). Asterisks indicate Bonferroni's post-test, sham-control vehicle-treated versus epileptic vehicle-treated $P = 0.0193$; epileptic vehicle-treated versus epileptic ICA-121431-treated $P = 0.0057$. (**G**–**J**) Results of the NOR test. (**G** and **H**) Representative examples of sessions with tracking data in sham-control and epileptic animals with vehicle application (**G**) and ICA-121431 application (**H**), respectively. Occupancy times are colour-coded (for calibration see scale bar). (**I**) The DI indicating if mice preferentially explore an object during the acquisition session. The DI was close to zero, indicating that mice did not discriminate the two objects in any group (no differences between groups, two-way ANOVA, n.s.). (**J**) DI in the NOR session. In all groups, animals discriminated the novel object. There were no differences between groups (two-way ANOVA, n.s.). (**K**) Schematic representation of Y-maze arena. (**L**) the number of arm entries was significantly higher in epileptic animals treated with vehicle [two-way ANOVA main effect, vehicle versus ICA-121431: $F(1,44) = 7.46$, $P = 0.0090$; sham-control versus epileptic: $F(1,44) = 8.47$, $P = 0.0056$; interaction: $F(1,44) = 0.29$, $P = 0.059$, Bonferroni's post tests indicated with asterisks, sham-control vehicle-treated versus epileptic vehicle-treated $P = 0.043$]. (**M**) Alternation scores. Significant Bonferroni's post-tests indicated with asterisks, $P = 0.03$. For these experiments we used sham-control vehicle-treated ($n = 14$), sham-control ICA-121431-treated ($n = 9$), epileptic vehicle-treated ($n = 16$) and epileptic ICA-121431-treated mice ($n = 9$).

phenomenon. It is nonetheless likely that changes in inhibitory circuits act together with degraded specificity of dendritic spikes to compromise the precision of CA1 firing.

Could the upregulation of dendritic Na_v channels be therapeutically targeted to treat cognitive comorbidities of chronic epilepsy? Several avenues have been shown to be potentially feasible. Despite the high degree of structural similarity between individual Na^+ channel isoforms, selective antagonists for specific Na^+ channel subunits have been developed, including for $\text{Na}_\text{v}1.3$.[18] In addition, antisense oligonucleotides could be used to selectively inhibit $\text{Na}_\text{v}1.3$ expression, potentially in a cell-type specific manner.[52,53] The availability of anticonvulsants that inhibit other, non-$\text{Na}_\text{v}1.3$ Na^+ channel isoforms, such as S-Lic, and have a proven efficacy against partial seizures may also allow us to combine blockers affecting abnormal dendritic spiking versus somatic action potential firing. In addition to applying selective Na_v channel modulators, the biological mechanisms leading to enhanced expression of specific Na_v channels could also be targeted. One mechanism underlying upregulation of $\text{Na}_\text{v}1.3$ in acquired experimental epilepsy is a GAPDH-mediated posttranscriptional regulation.[28] Importantly, this upregulation is ameliorated by a ketogenic diet, which is used to control therapy-refractory epilepsies in children.[28] In addition, the anticonvulsant valproic acid has been shown to epigenetically reduce $\text{Na}_\text{v}1.3$ expression via promoter methylation.[54] Thus, several avenues for direct modulation of Na_v channels or regulation of their expression levels may be exploited to correct epilepsy-induced Na_v channel overexpression, and to reverse cognitive impairments in chronic TLE.

Acknowledgements

We are very grateful to David Greenberg, Jason Kerr and Damian Wallace for technical help and advice, as well as the supply of analysis algorithms. We gratefully acknowledge the support of Jonathan Ewell in editing the manuscript. We are grateful to Lea Keller for technical support, and Thoralf Opitz for support with animal husbandry and *in vivo* pharmacology. We acknowledge the support of the Imaging Core Facility of the Bonn Technology Campus Life Sciences funded by the Deutsche Forschungsgemeinschaft (DFG, German Research Foundation), Projektnummer 388169927.

Funding

The work was supported by the SFB 1089 (to H.B., S.B. and C.H.); the Research Group FOR2715 (to T.K. and H.B.) and SPP 2041 (to H.B.); EXC 2151 under Germany's Excellence Strategy (to H.B.); and BL 767/5-1 (to S.B.), all funded by programs of the Deutsche Forschungsgemeinschaft (DFG, German Research Foundation); and support of the Humboldt Foundation PSI (to K.G.). A.N.H. was supported by the IMPRS Brain and Behaviour.

Competing interests

N.M. was partially financed by BIAL. BIAL was not involved in the conception, planning, writing or publication of the study. The other authors report no competing interests.

Supplementary material

Supplementary material is available at *Brain* online.

References

1. Losonczy A, Magee JC. Integrative properties of radial oblique dendrites in hippocampal CA1 pyramidal neurons. *Neuron*. 2006;50:291-307.
2. Losonczy A, Makara JK, Magee JC. Compartmentalized dendritic plasticity and input feature storage in neurons. *Nature*. 2008; 452:436-441.
3. Bittner KC, Grienberger C, Vaidya SP, *et al*. Conjunctive input processing drives feature selectivity in hippocampal CA1 neurons. *Nat Neurosci*. 2015;18:1133-1142.
4. Sheffield ME, Dombeck DA. Calcium transient prevalence across the dendritic arbour predicts place field properties. *Nature*. 2015;517:200-204.
5. Bernard C, Anderson A, Becker A, Poolos NP, Beck H, Johnston D. Acquired dendritic channelopathy in temporal lobe epilepsy. *Science*. 2004;305:532-535.
6. Becker AJ, Pitsch J, Sochivko D, *et al*. Transcriptional upregulation of Cav3.2 mediates epileptogenesis in the pilocarpine model of epilepsy. *J.Neurosci*. 2008;28:13341-13353.

7. Su H, Sochivko D, Becker A, *et al*. Upregulation of a T-type Ca^{2+} channel causes a long-lasting modification of neuronal firing mode after status epilepticus. *J Neurosci*. 2002;22:3645-3655.
8. Jung S, Bullis JB, Lau IH, Jones TD, Warner LN, Poolos NP. Downregulation of dendritic HCN channel gating in epilepsy is mediated by altered phosphorylation signaling. *J Neurosci*. 2010;30:6678-6688.
9. Jung S, Jones TD, Lugo JNJ, *et al*. Progressive dendritic HCN channelopathy during epileptogenesis in the rat pilocarpine model of epilepsy. *J Neurosci*. 2007;27:13012-13021.
10. Royeck M, Kelly T, Opitz T, *et al*. Downregulation of spermine augments dendritic persistent sodium currents and synaptic integration after status epilepticus. *J Neurosci*. 2015;35: 15240-15253.
11. Li F, Liu L. Comparison of kainate-induced seizures, cognitive impairment and hippocampal damage in male and female mice. *Life Sci*. 2019;232:116621.
12. Twele F, Töllner K, Brandt C, Löscher W. Significant effects of sex, strain, and anesthesia in the intrahippocampal kainate mouse model of mesial temporal lobe epilepsy. *Epilepsy Behav*. 2016;55:47-56.
13. Dana H, Chen TW, Hu A, *et al*. Thy1-GCaMP6 transgenic mice for neuronal population imaging *in vivo*. *PLoS One*. 2014;9:e108697.
14. Bedner P, Dupper A, Hüttmann K, *et al*. Astrocyte uncoupling as a cause of human temporal lobe epilepsy. *Brain*. 2015;138(Pt 5): 1208-1222.
15. Doeser A, Dickhof G, Reitze M, *et al*. Targeting pharmacoresistant epilepsy and epileptogenesis with a dual-purpose antiepileptic drug. *Brain*. 2015;138(Pt 2):371-387.
16. Soares-da-Silva P, Pires N, Bonifacio MJ, Loureiro AI, Palma N, Wright LC. Eslicarbazepine acetate for the treatment of focal epilepsy: An update on its proposed mechanisms of action. *Pharmacol Res Perspect*. 2015;3:e00124.
17. Holtkamp D, Opitz T, Hebeisen S, Soares-da-Silva P, Beck H. Effects of eslicarbazepine on slow inactivation processes of sodium channels in dentate gyrus granule cells. *Epilepsia*. 2018;59: 1492-1506.
18. McCormack K, Santos S, Chapman ML, *et al*. Voltage sensor interaction site for selective small molecule inhibitors of voltage-gated sodium channels. *Proc Natl Acad Sci USA*. 2013; 110:E2724-E2732.
19. Golding NL, Staff NP, Spruston N. Dendritic spikes as a mechanism for cooperative long-term potentiation. *Nature*. 2002;418:326-331.
20. Royer S, Zemelman BV, Losonczy A, *et al*. Control of timing, rate and bursts of hippocampal place cells by dendritic and somatic inhibition. *Nat Neurosci*. 2012;15:769-775.
21. Greenberg DS, Kerr JND. Automated correction of fast motion artifacts for two-photon imaging of awake animals. *J Neurosci Methods*. 2009;176:1-15.
22. Pnevmatikakis EA, Soudry D, Gao Y, *et al*. Simultaneous denoising, deconvolution, and demixing of calcium imaging data. *Neuron*. 2016;89:285-299.
23. Danielson NB, Kaifosh P, Zaremba JD, *et al*. Distinct contribution of adult-born hippocampal granule cells to context encoding. *Neuron*. 2016;90:101-112.
24. Bui AD, Nguyen TM, Limouse C, *et al*. Dentate gyrus mossy cells control spontaneous convulsive seizures and spatial memory. *Science*. 2018;359:787-790.
25. Bragin A, Engel JJ, Wilson CL, Vizentin E, Mathern GW. Electrophysiologic analysis of a chronic seizure model after unilateral hippocampal KA injection. *Epilepsia*. 1999;40:1210-1221.
26. Remy S, Csicsvari J, Beck H. Activity-dependent control of neuronal output by local and global dendritic spike attenuation. *Neuron*. 2009;61:906-916.
27. Schmidt S, Pothmann L, Müller-Komorowska D, Opitz T, Da Soares Silva P, Beck H. Complex effects of eslicarbazepine on inhibitory micro networks in chronic experimental epilepsy. *Epilepsia*. 2021;62:542-556.
28. Lin G-W, Lu P, Zeng T, *et al*. GAPDH-mediated posttranscriptional regulations of sodium channel Scn1a and Scn3a genes under seizure and ketogenic diet conditions. *Neuropharmacology*. 2017;113:480-489.
29. Lenck-Santini PP, Holmes GL. Altered phase precession and compression of temporal sequences by place cells in epileptic rats. *J Neurosci*. 2008;28:5053-5062.
30. Zhou JL, Lenck-Santini PP, Holmes GL. Postictal single-cell firing patterns in the hippocampus. *Epilepsia*. 2007;48:713-719.
31. Shuman T, Aharoni D, Cai DJ, *et al*. Breakdown of spatial coding and interneuron synchronization in epileptic mice. *Nat Neurosci*. 2020;23:229-238.
32. Ewell LA, Fischer KB, Leibold C, Leutgeb S, Leutgeb JK. The impact of pathological high-frequency oscillations on hippocampal network activity in rats with chronic epilepsy. *Elife*. 2019;8: e42148.
33. Danielson NB, Zaremba JD, Kaifosh P, Bowler J, Ladow M, Losonczy A. Sublayer-specific coding dynamics during spatial navigation and learning in hippocampal area CA1. *Neuron*. 2016;91:652-665.
34. Zhou JL, Lenck-Santini PP, Zhao Q, Holmes GL. Effect of interictal spikes on single-cell firing patterns in the hippocampus. *Epilepsia*. 2007;48:720-731.
35. Muldoon SF, Villette V, Tressard T, *et al*. GABAergic inhibition shapes interictal dynamics in awake epileptic mice. *Brain: A Journal of Neurology*. 2015;138(Pt 10):2875-2890.
36. Wilson DE, Whitney DE, Scholl B, Fitzpatrick D. Orientation selectivity and the functional clustering of synaptic inputs in primary visual cortex. *Nat Neurosci*. 2016;19:1003-1009.
37. Muller C, Beck H, Coulter D, Remy S. Inhibitory control of linear and supralinear dendritic excitation in CA1 pyramidal neurons. *Neuron*. 2012;75:851-864.
38. Makara JK, Losonczy A, Wen Q, Magee JC. Experience-dependent compartmentalized dendritic plasticity in rat hippocampal CA1 pyramidal neurons. *Nat Neurosci*. 2009;12: 1485-1487.
39. Kelly T, Beck H. Functional properties of granule cells with hilar basal dendrites in the epileptic dentate gyrus. *Epilepsia*. 2017;58: 160-171.
40. O'Keefe J, Nadel L. *The hippocampus as a cognitive map*. Oxford University Press; 1978.
41. Sheffield ME, Dombeck DA. Dendritic mechanisms of hippocampal place field formation. *Curr Opin Neurobiol*. 2019;54:1-11.
42. Sheffield MEJ, Adoff MD, Dombeck DA. Increased prevalence of calcium transients across the dendritic arbor during place field formation. *Neuron*. 2017;96:490-504.e5.
43. Basak R, Narayanan R. Spatially dispersed synapses yield sharply-tuned place cell responses through dendritic spike initiation. *J Physiol (Lond)*. 2018;596:4173-4205.
44. Karnam HB, Zhou J-L, Huang L-T, Zhao Q, Shatskikh T, Holmes GL. Early life seizures cause long-standing impairment of the hippocampal map. *Exp Neurol*. 2009;217:378-387.
45. Basak R, Narayanan R. Robust emergence of sharply tuned place-cell responses in hippocampal neurons with structural and biophysical heterogeneities. *Brain Struct Funct*. 2020;225: 567-590.
46. Chen C, Westenbroek RE, Xu X, *et al*. Mice lacking sodium channel beta1 subunits display defects in neuronal excitability, sodium channel expression, and nodal architecture. *J Neurosci*. 2004;24:4030-4042.

47. Cummins TR, Aglieco F, Renganathan M, Herzog RI, Dib-Hajj SD, Waxman SG. Nav1.3 sodium channels: Rapid repriming and slow closed-state inactivation display quantitative differences after expression in a mammalian cell line and in spinal sensory neurons. *J Neurosci*. 2001;21:5952-5961.
48. Spratt PWE, Ben-Shalom R, Keeshen CM, *et al*. The autism-associated gene Scn2a contributes to dendritic excitability and synaptic function in the prefrontal cortex. *Neuron*. 2019;103:673-685.e5.
49. Pothmann L, Klos C, Braganza O, *et al*. Altered dynamics of canonical feedback inhibition predicts increased burst transmission in chronic epilepsy. *J Neurosci*. 2019;39: 8998-9012.
50. Lopez-Pigozzi D, Laurent F, Brotons-Mas JR, *et al*. Altered oscillatory dynamics of CA1 parvalbumin basket cells during theta–gamma rhythmopathies of temporal lobe epilepsy. *eNeuro*. 2016;3:ENEURO.0284–16.2016.
51. Valero M, Averkin RG, Fernandez-Lamo I, *et al*. Mechanisms for selective single-cell reactivation during offline sharp-wave ripples and their distortion by fast ripples. *Neuron*. 2017;94:1234-1247.e7.
52. Lenk GM, Jafar-Nejad P, Hill SF, *et al*. Scn8a antisense oligonucleotide is protective in mouse models of SCN8A encephalopathy and Dravet syndrome. *Ann Neurol*. 2020;87:339-346.
53. Han Z, Chen C, Christiansen A, *et al*. Antisense oligonucleotides increase Scn1a expression and reduce seizures and SUDEP incidence in a mouse model of Dravet syndrome. *Sci Transl Med*. 2020;12:eaaz6100.
54. Tan N-N, Tang H-L, Lin G-W, *et al*. Epigenetic downregulation of Scn3a expression by valproate: A possible role in its anticonvulsant activity. *Mol Neurobiol*. 2017;54:2831-2842.